Thermodynamic Optimization of the Ca-Fe-O System

TAUFIQ HIDAYAT, DENIS SHISHIN, SERGEI A. DECTEROV, and EVGUENI JAK

The present study deals with the thermodynamic optimization of the Ca-Fe-O system. All available phase equilibrium and thermodynamic experimental data are critically assessed to obtain a self-consistent set of model parameters for the Gibbs energies of all stoichiometric and solution phases. Model predictions of the present study are compared with previous assessments. Wüstite and lime are described as one monoxide solution with a miscibility gap, using the random mixing Bragg-Williams model. The solubility of CaO in the "Fe_3O_4" magnetite (spinel) phase is described using the sublattice model based on the Compound Energy Formalism. The effect of CaO on the stability of the spinel phase is evaluated. The liquid CaO-FeO-Fe_2O_3 slag is modeled using the Modified Quasichemical Formalism. Liquid metal phase is described as a separate solution by an associate model.

I. INTRODUCTION

THE CaO-FeO-Fe_2O_3 portion of the Ca-Fe-O system is one of the essential subsystems for many metallurgical processes, including iron ore sintering, copper-making industry, and iron- and steel-making processes. The thermodynamic description of the solubility of oxygen in the Fe-Ca alloys is important for the deoxidation of steel.

Comprehensive assessments of the Ca-Fe-O system are available in the literature.[1,2] Very good results were obtained; however, some previously existing[3,4] and new experimental data[4–6] were not taken into account in these studies. As a result, there is a discrepancy between model predictions and these experimental data. Furthermore, the oxygen content in the Fe-Ca liquid metal was not assessed. The purpose of the present study is to obtain a thermodynamic database capable of describing all experimental data available up-to-date. In order to achieve that, a thermodynamic optimization of the system is performed. The first step is selecting the appropriate thermodynamic models for all phases in the system. Then, a critical and simultaneous evaluation/assessment of all available thermodynamic and phase diagram data is performed. Finally, the thermodynamic model parameters are optimized in order to obtain one self-consistent set of model equations for the Gibbs energies of all phases, best reproducing the experimental data as functions of temperature and composition.

The list of the stable phases, models, and notations used in the present study is given in Table I.

Thermodynamic properties and phase diagrams can be back-calculated from the model equations. Thermodynamic property data, such as enthalpies and activities, can aid in assessing phase diagrams, and phase diagram measurements can be used to derive the thermodynamic properties. The described procedure is sometimes referred to as Calphad technique.

The present thermodynamic optimization has been performed using the FactSage thermodynamic software package[7] as a part of the development of a self-consistent thermodynamic database for the Al-Ca-Cu-Fe-Mg-Si-O-S multi-components system.

II. BINARY SUBSYSTEMS

A. Fe-O

The assessment of the Fe-O system was reported earlier.[8,9] In the present study, the properties of solid phases were adopted from Hidayat et al.[8] and the properties of slag and liquid metal are from Shishin et al.[9] The assessed phase diagram is presented in Figure 1. It may be compared with model predictions of Selleby and Sundman.[2]

B. Ca-O

The available experimental data on the Ca-O system are very limited. Bevan and Richardson[10] studied the mixtures of Ca and CaO. They observed the full solubility of CaO particles in Ca at 1523 K (1250 °C) up to 20 mol pct CaO. Making a correction for the final size of lime particles, they suggested that the solubility of lime in Ca is 15 to 18 mol pct. The measured eutectic

TAUFIQ HIDAYAT, Research Fellow, DENIS SHISHIN, Postdoctoral Research Fellow, and EVGUENI JAK, Professor, are with the Pyrometallurgical Research Laboratory, PYROSEARCH, School of Chemical Engineering, The University of Queensland, Brisbane, Australia. Contact e-mail: t.hidayat@uq.edu.au SERGEI A. DECTEROV, Research Professor, is with the Center for Research in Computational Thermochemistry (CRCT), Dép. de Génie Chimique, École Polytechnique, Montréal, Canada and Honorary Professor, School of Chemical Engineering, The University of Queensland, Brisbane, QLD, Australia.
Manuscript submitted May 14, 2013.
Article published online November 16, 2015.

Table I. Stable Oxide and Metallic Phases in the Ca-Fe-O System at Ambient Total Pressure

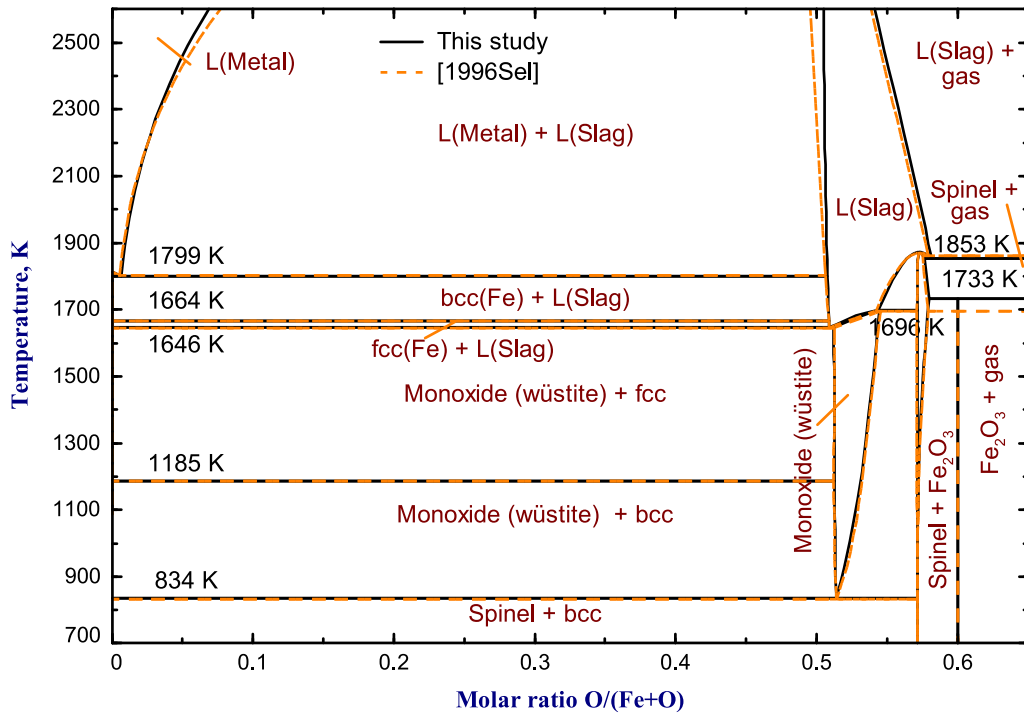| Phase	Model	Short Notation Used in this Study
Hematite	stoichiometric compound	Fe_2O_3
$CaFe_2O_4$	stoichiometric compound	CF
$Ca_2Fe_2O_5$	stoichiometric compound	C2F
$CaFe_3O_5$	stoichiometric compound	CWF
$CaFe_4O_7$	stoichiometric compound	CF2
$CaFe_5O_7$	stoichiometric compound	CW3F
$Ca_4Fe_9O_{17}$	stoichiometric compound	C4WF4
$Ca_4Fe_{17}O_{29}$	stoichiometric compound	C4WF8
Spinel	$(Fe^{2+}, Fe^{3+})^T [Fe^{2+}, Fe^{3+}, Ca^{2+}, Va]_2^\circ O_4^{2-}$	Sp
Wüstite-Lime solid solution	$(FeO, FeO_{1.5}, CaO)$	monoxide, mono1—wüstite side, mono2—lime side
Slag (liquid oxide)	$(Fe^{2+}, Fe^{3+}, Ca^{2+})(O^{2-})$	L(slag)
Liquid metal	(Fe, O, Ca, CaO)	L(metal)
fcc	(Fe, Ca)	fcc
bcc	(Fe, Ca)	bcc

Fig. 1—Phase diagram of the Fe-O system at total pressure of 1 atm: solid lines are calculated in this study, and dashed lines are calculated using the database of the previous study.[2]

temperature between Ca and CaO was 1106 K to 1109 K (833 °C to 836 °C).[10] In the assessment of Wriedt,[11] lower solubility of CaO in Ca than reported by Bevan and Richardson[10] by was suggested (Figure 2). According to Wriedt,[11] higher solubility would result in a very low eutectic temperature. In the present study, the evaluated phase diagram is similar to the assessment of Wriedt[11] and closer to the experimental points than the model predictions of Selleby and Sundman.[2]

C. Ca-Fe

The phase diagram of the Ca-Fe system has been assessed by Anglezio et al.[12] Their evaluation was accepted in the present study. The solubility of Ca in the

iron-rich phases, bcc, fcc, and liquid, is very small. The solubility of Fe in the Ca-rich phases, fcc, bcc, and liquid, is unknown, but should be also small. The calculated phase diagram near the Fe corner is shown in Figure 3. The model predictions of Selleby and Sundman[2] give practically the same results and are not shown in Figure 3.

III. THERMODYNAMIC MODELS

A. Stoichiometric Compounds

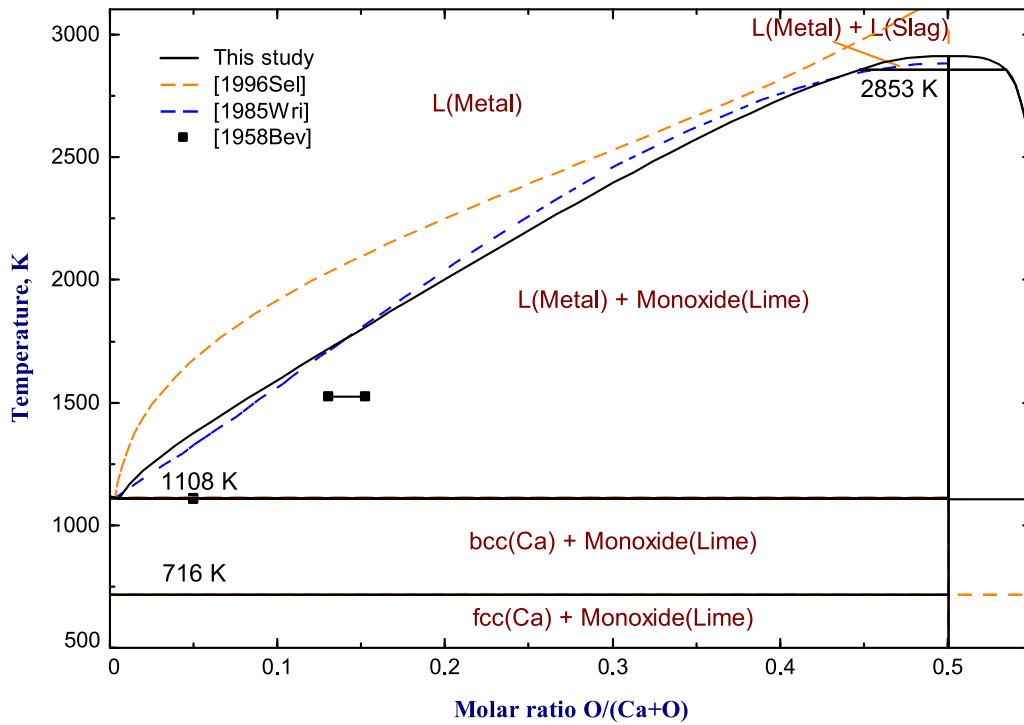Many solid phases in the present study are treated as stoichiometric compounds (Table I). Their Gibbs

Fig. 2—Phase diagram of the Ca-O system: solid lines are calculated in this study, dashed lines are assessments of earlier studies,[2,11] and points are experimental data.[10] Gas phase is suppressed.
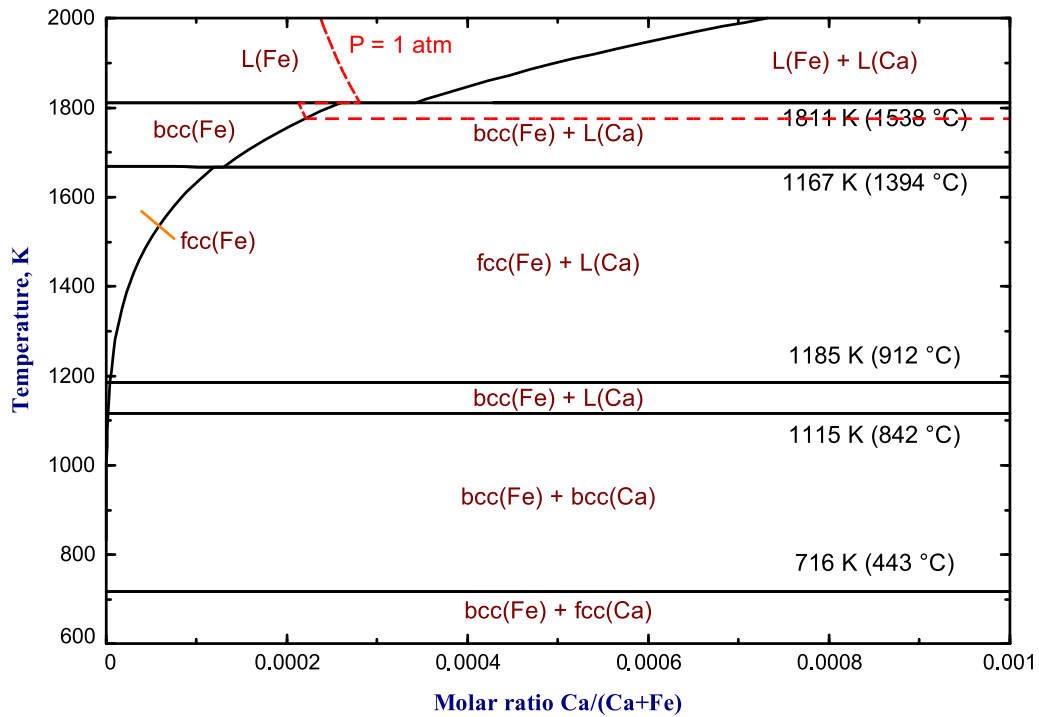

Fig. 3—Phase diagram of the Fe-Ca system close to the iron corner. Dashed line shows the formation of the gas phase at a total pressure of 1 atm.

energies are independent of composition. The Gibbs energy of formation of a compound from elements in their standard state at a temperature of T (K) and a pressure of 1 atm is given by

$$\Delta G = \Delta H_{298.15}^{\circ} - T S_{298.15}^{\circ} + \int_{298.15}^{T} C_P(T)\mathrm{d}T \\ - T \int_{298.15}^{T} \frac{C_P(T)}{T}\mathrm{d}T, \qquad [1]$$

where $\Delta H_{298.15}^{\circ}$ is the standard enthalpy of formation at 298.15 K (25 °C), $S_{298.15}^{\circ}$ is the standard entropy at 298.15 K (25 °C), and $C_P(T)$ is the molar heat capacity.

B. Monoxide

Wüstite $Fe_{1-x}O$ has a range of non-stoichiometry towards oxygen[8] and a partial mutual solubility with lime (CaO). This solid solution was modeled as a random mixture of Fe^{2+}, Fe^{3+}, and Ca^{2+} ions on cation sites with simple polynomial excess Gibbs energy terms. It is assumed that cation vacancies remain associated with Fe^{3+} ions to comply with the local charge balance condition and thus do not contribute to the configurational entropy. This approach is discussed in detail in Hidayat et al.[8] The Gibbs energy per mole of components FeO, $FeO_{1.5}$ and CaO is given by

$$g = (X_{FeO}g_{FeO}^{\circ} + X_{FeO_{1.5}}g_{FeO_{1.5}}^{\circ} + X_{CaO}g_{CaO}^{\circ}) \\ + RT(X_{FeO}\ln X_{FeO} + X_{FeO_{1.5}}\ln X_{FeO_{1.5}} + X_{CaO}\ln X_{CaO}) \\ + X_{FeO}X_{FeO_{1.5}}L_{FeO,FeO_{1.5}} + X_{CaO}X_{FeO_{1.5}}L_{CaO,FeO_{1.5}} \\ + X_{CaO}X_{FeO}L_{CaO,FeO} \qquad [2]$$

where g_M° is the Gibbs energy of pure component M and X_M is the mole fraction. The interaction energy $L_{M,N}$ between components M and N is expanded as a polynomial in the mole fractions of the components:

$$L_{M,N} = \sum_{i,j \geq 0} q_{M,N}^{ij} X_M^i X_N^j, \qquad [3]$$

where $q_{M,N}^{ij}$ are the binary model parameters. No ternary terms were used in the present study. The binary terms are extrapolated into the ternary system using the Kohler method.[13]

C. Spinel

Ca is soluble in magnetite, Fe_3O_4, which has a cubic spinel structure.

The model for spinel was developed within the framework of the Compound Energy Formalism (CEF). The structure of spinel may be derived from the fcc close packing of oxygen anions. Cations occupy half of the octahedral interstices and one-eighth of the tetrahedral interstices.[14] It is a common practice to distinguish tetrahedral and octahedral sublattices and represent spinels as $(A, B, \ldots)^{tetr}[A, B, \ldots]_2^{oct}O_4$, where A, B, etc., are cations with charges $+2$ and $+3$, rarely $+4$

or $+1$. Oxygen has a charge of -2. The condition of electroneutrality must be always respected.

The Gibbs energy expression in the CEF per formula unit is[15,16]

$$g = \sum_i \sum_j Y_i' Y_j'' G_{ij} - T S^{config} + g^E, \qquad [4]$$

where Y_i' and Y_j'' represent the site fractions of constituents i and j on the first and second sublattices, respectively, G_{ij} is the Gibbs energy of a pseudocomponent $(i)[j]_2O_4$, S^{config} is the configurational entropy,

$$S^{config} = -R\left(\sum_i Y_i' \ln Y_i' + 2\sum_j Y_j'' \ln Y_j''\right), \qquad [5]$$

and g^E is the excess Gibbs energy, which was set to zero in the present study.

The non-stoichiometry of spinel towards excess oxygen was modeled in Reference 14 by introducing neutral vacancies (Va) on the octahedral sublattice. Taking vacancies into account, the model for spinel in the Ca-Fe-O system is based on the following formula unit:

$$(Fe^{2+}, Fe^{3+})^{tetr}[Ca^{2+}, Fe^{2+}, Fe^{3+}, Va]_2^{oct}O_4^{-2} \qquad [6]$$
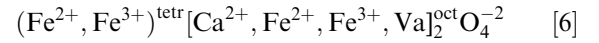
The Ca^{2+} cations were introduced only on the octahedral sites for two reasons. First of all, it is well known that compounds such as $CaFe_2O_4$, $CaAl_2O_4$, and $CaCr_2O_4$ do not have the spinel crystal structures, presumably because relatively large Ca^{2+} cations cannot be squeezed into small tetrahedral sites. Secondly, the solubility of Ca^{2+} is found to be much higher in Fe_3O_4 than in $FeAl_2O_4$, which may be explained by the fact that Fe_3O_4 is an inverse spinel and divalent cations (Fe^{2+}) on the octahedral sites can be replaced by Ca^{2+}; the hercynite ($FeAl_2O_4$) is a normal spinel, and Ca^{2+} should substitute Fe^{2+} on tetrahedral sites. It is argued that if it was possible for calcium to replace Fe^{2+} on tetrahedral site, the solubility of Ca^{2+} in $FeAl_2O_4$ would be of the same order as that in Fe_3O_4.

The introduction of Ca^{2+} only on the octahedral sites results in only two additional end-members: $\left[(Fe^{3+})^{tetr}[Ca^{2+}]_2^{oct}O_4^{-2}\right]^{-1}$ and $\left[(Fe^{2+})^{tetr}[Ca^{2+}]_2^{oct}O_4^{-2}\right]^{-2}$. The Gibbs energies of these end-members can be obtained from two equations:

$$G_{(Fe^{3+})^{tetr}[Ca_{0.5}^{2+}, Fe_{0.5}^{3+}]_2^{oct}O_4^{-2}} = 0.5 G_{(Fe^{3+})^{tetr}[Fe^{3+}]_2^{oct}O_4^{2-}} \\ + 0.5 G_{(Fe^{3+})^{tetr}[Ca^{2+}]_2^{oct}O_4^{2-}} - T S^{mix} \qquad [7]$$

where $S^{mix} = -2R\ln 0.5$, and

$$\Delta_{Fe^{3+}Fe^{2+}:Fe^{2+}Ca^{2+}} = G_{(Fe^{3+})^{tetr}[Ca^{2+}]_2^{oct}O_4^{-2}} \\ + G_{(Fe^{2+})^{tetr}[Fe^{2+}]_2^{oct}O_4^{-2}} - G_{(Fe^{3+})^{tetr}[Fe^{2+}]_2^{oct}O_4^{2-}} \\ - G_{(Fe^{2+})^{tetr}[Ca^{2+}]_2^{oct}O_4^{-2}} \qquad [8]$$

In this study, the model parameter $\Delta_{Fe^{3+}Fe^{2+}:Fe^{2+}Ca^{2+}}$ is set to zero and the solubility of Ca^{2+} in spinel can be modeled optimizing only the Gibbs energy of the hypothetical neutral inverse spinel: $(Fe^{3+})^{tetr}[Ca_{0.5}^{2+}, Fe_{0.5}^{3+}]_2^{oct}O_4^{-2}$. The

heat capacity of this spinel is approximated to be the same as for calcium ferrite, $CaFe_2O_4$, while the enthalpy of formation and entropy are variable parameters.

D. fcc and bcc

Both iron and calcium can exist in an fcc and bcc structures, but they are only partially miscible in each other. The Bragg–Williams model that assumes random mixing of atoms was used for fcc and bcc solid solutions. The Gibbs energy per mole of atoms is given by

$$g = (X_{Ca}g_{Ca}^{\circ} + X_{Fe}g_{Fe}^{\circ}) + RT(X_{Ca} \ln X_{Ca} + X_{Fe} \ln X_{Fe}) + X_{Ca}X_{Fe}L_{Ca,Fe}, \qquad [9]$$

where g_M° is the Gibbs energy of pure component M and X_M is the mole fraction. The interaction energy $L_{Ca,Fe}$ between components M and N is expanded as a Redlich–Kister polynomial:

$$L_{Ca,Fe} = \sum_{i \geq 0} L_{Ca,Fe}^i (X_{Ca} - X_{Fe})^i, \qquad [10]$$

where $L_{Ca,Fe}^i$ are the binary model parameters that can be temperature-dependent. Contrary to calcium, there exist magnetic transitions in fcc and bcc. The contributions of the magnetic transitions to the thermodynamic functions of the Fe-Ca solid alloys were described using the method proposed by Hillert and Jarl.[17] Critical temperature, T_C, and magnetic constant, β, were interpolated linearly between values for Fe and zero for calcium.

E. Liquid Oxide (Slag)

The liquid oxide phase is an ionic melt where metal cations are predominantly surrounded by oxygen anions. In other words, there is almost full first-nearest-neighbor (FNN) short-range ordering (SRO) between cations and anions. Furthermore, there is a strong tendency for second-nearest-neighbor SRO of some cations in melts. In particular, basic cations such as Ca^{2+} form strong second-nearest-neighbor (SNN) pairs with acidic cations such as Si^{+4}. The effects of both FNN and SNN SRO are described by the Modified Quasichemical Model (MQM).[18,19] Even though in the CaO-FeO-Fe_2O_3 slag, SNN ordering is not very strong, the present model is used with a vision to develop a broader database for calculations in multicomponent systems, including SiO_2.

To explain the meaning of the parameters, let us consider the binary system Fe_2O_3-CaO as an example. The most significant parameter of the MQM model is the Gibbs energy of the corresponding pair exchange reaction:

$$(Ca^{2+}\text{-}Ca^{2+}) + (Fe^{3+}\text{-}Fe^{3+}) = 2(Ca^{2+}\text{-}Fe^{3+}); \\ \Delta g_{Ca^{2+},Fe^{3+}}, \qquad [11]$$
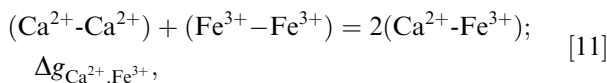
where $(Ca^{2+}\text{-}Fe^{3+})$ represents a second-nearest-neighbor pair. The molar Gibbs energy of the solution is given by[19]

$$g = (X_{FeO_{1.5}}g_{FeO_{1.5}}^{\circ} + X_{CaO}g_{CaO}^{\circ}) - T\Delta S^{config} \\ + X_{Fe^{3+}Ca^{2+}}(\Delta g_{Ca^{2+}Fe^{3+}}/2), \qquad [12]$$

where X_i and g_i° are the mole fractions and molar Gibbs energies of the components and $X_{Fe^{3+}Ca^{2+}}$ is the mole fraction of Ca^{2+}-Fe^{3+} pairs at equilibrium. ΔS^{config} is the configuration entropy, the expression for which is given elsewhere.[18,19]

Δg_{AB} can be expanded as an empirical polynomial in terms of equivalent component fractions

$$\Delta g_{AB} = \Delta g_{AB}^{\circ} + \sum_{(i+j) \geq 1} q_{AB}^{ij} Y_A^i Y_B^j, \qquad [13]$$

where Δg_{AB}° and q_{AB}^{ij} are empirical binary coefficients which may be functions of temperature and pressure. Y_m are "coordination-equivalent" fractions, which are defined as

$$Y_m = Z_m n_m / \sum_i Z_i n_i, \qquad [14]$$

where n_m and Z_m are the number of moles and the coordination number of the component m, respectively. The composition of maximum short-range ordering is determined by the ratio of the coordination numbers, which was explained in detail earlier.[18]

A symmetric Kohler model was previously used[20] for the interpolation of CaO-FeO, FeO-$FeO_{1.5}$, and CaO-$FeO_{1.5}$ binary parameters into the ternary system. In the present study, the Kohler/Toop extrapolation[19] with $FeO_{1.5}$ as an "asymmetric component" is selected to achieve a better description of the experimental data in the CaO-FeO-Fe_2O_3 system. This is equivalent to treating $FeO_{1.5}$ as an "amphoteric" component, as opposed to CaO and FeO which are "basic" components.

Ternary parameters are also used in the present study to better describe the experimental data. The ternary parameters, $q_{A,B(C)}^{ijk}$, are the effects of the presence of the third component C upon binary interactions between components A and B. The formulae are given elsewhere.[19]

F. Liquid Metal

The model for the liquid metal assumes random mixing of components and associates on one sublattice:

$$(Fe, Ca, O, CaO) \qquad [15]$$
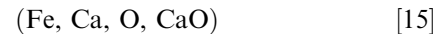
The molar Gibbs energy is given by

$$g = \sum_i X_i g_i^{\circ} + RT \sum_i X_i \ln X_i + g^{excess}, \qquad [16]$$

where X_i are the molar fractions of components and g_i° are the standard Gibbs energies of pure components. The molar excess Gibbs energy of a binary system with components A and B is expressed as

$$g_{AB}^{excess} = \alpha_{AB} X_A X_B, \qquad [17]$$

where α_{AB} parameter may be expanded in a Redlich–Kister form:

$$\alpha_{AB} = \sum_{i \geq 0} L_{AB}^i (X_A - X_B)^i \qquad [18]$$

The interpolation of binary terms into ternary subsystems is done using the Muggianu method.[13]

IV. ASSESSMENT OF EXPERIMENTAL DATA

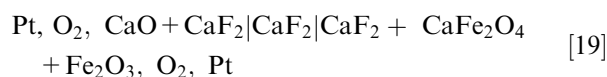### A. Thermodynamic Properties of Stoichiometric Compounds

Figures 4 and 5 show the compositions of ternary compounds in the Ca-Fe-O system: $Ca_2Fe_2O_5$ (C2F), $CaFe_2O_4$ (CF), $CaFe_3O_5$ (CWF), $CaFe_5O_7$ (CW3F), and $Ca_4Fe_9O_{17}$ (C4WF4). The corresponding three-phase equilibria are calculated.

To fix the thermodynamic properties of these stoichiometric compounds, the heat capacity, $C_P(T)$, entropy, $S_{298.15}^{\circ}$, and enthalpy of formation, $\Delta H_{298.15}^{\circ}$, must be established.

For $CaFe_2O_4$ (CF), the low temperature $C_P(T)$ was measured by King[21] from 52.3 K to 298.16 K

($-220.7\ ^{\circ}$C to 25 $^{\circ}$C) using the adiabatic calorimetry. He extrapolated the heat capacity to 0 K ($-273\ ^{\circ}$C) and calculated the entropy at 298.15 K (25 $^{\circ}$C) using the third law to be $S_{298.15}^{\circ} = 145.2 \pm 0.8$ J mol^{-1} K^{-1}. Rajagopalan et al.[22] used a laser flash method to measure the heat capacity of $CaFe_2O_4$ from 297 K to 1091 K (24 $^{\circ}$C to 818 $^{\circ}$C). The obtained values were significantly higher than the sum of heat capacities of pure oxides and were not in agreement with the heat content data available from Bonnickson.[23] The latter measured the heat content of calcium ferrite samples over the temperature range from 411 K to 1805 K (138 $^{\circ}$C to 1532 $^{\circ}$C). His data are shown in Figure 6.

No direct measurements of the enthalpy of formation are available. The Gibbs energy of formation of $CaFe_2O_4$ from oxides was measured by Rezukhina and Bagin'ska,[24] by Jacob et al.[25] and by Forsberg et al.[26] All authors used the EMF cell:

$$\text{Pt, O}_2,\ \text{CaO} + \text{CaF}_2 | \text{CaF}_2 | \text{CaF}_2 +\ \text{CaFe}_2\text{O}_4 \\ + \text{Fe}_2\text{O}_3,\ \text{O}_2,\ \text{Pt} \qquad [19]$$

to measure the Gibbs energy of the reaction

$$\text{CaO} + \text{Fe}_2\text{O}_3 = \text{CaFe}_2\text{O}_4,\ \Delta G = -2FE \qquad [20]$$

The results are summarized in Figure 7. The data of Rezukhina and Bagin'ska[24] and Forsberg et al.[26] are in agreement but differ from that of Jacob et al.[25]
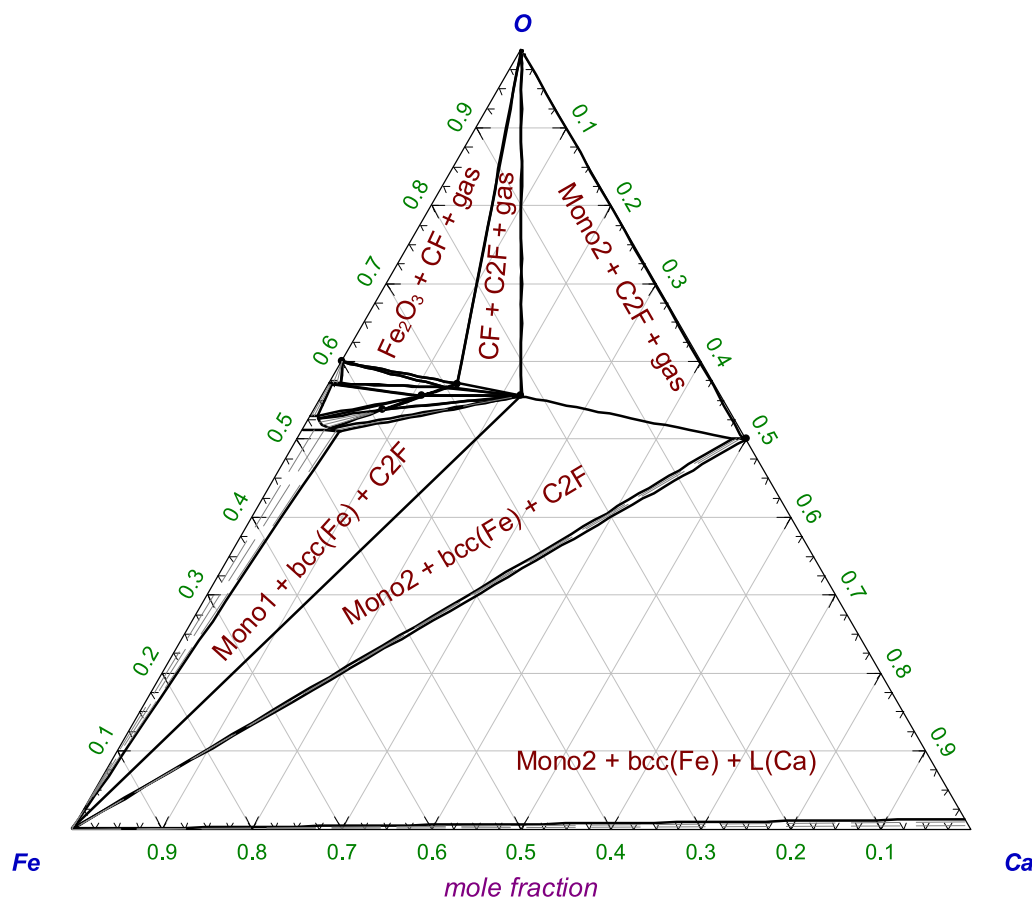

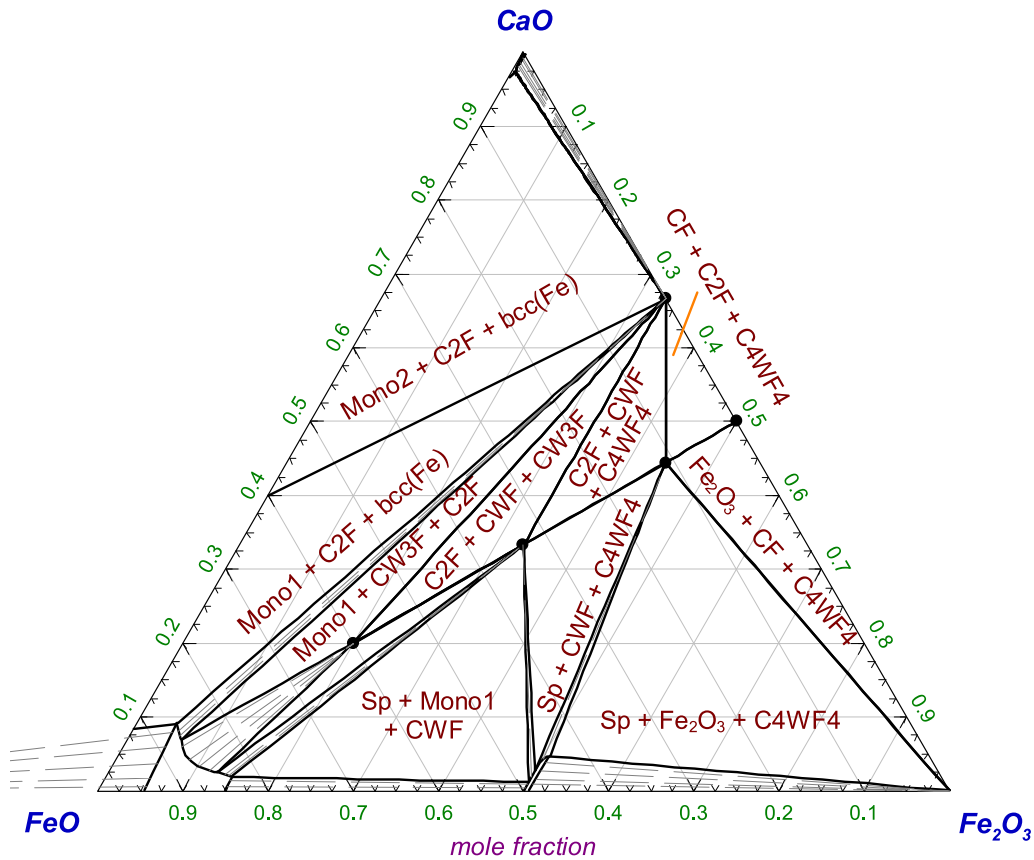Fig. 4—Phase diagram of the Ca-Fe-O system at 1173 K (900 °C) and total pressure of 1 atm.

Fig. 5—The CaO-FeO-Fe₂O₃ portion of the phase diagram of the Ca-Fe-O system at 1173 K (900 °C) and total pressure of 1 atm.
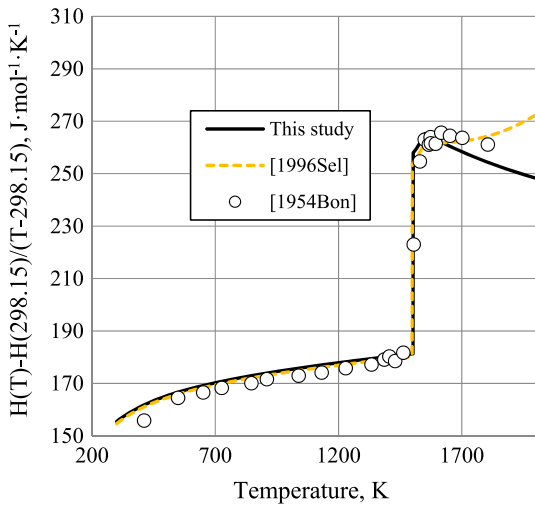

Fig. 6—Normalized heat content of CaFe₂O₄: experimental points[23] and calculated lines. Solid lines are calculations of the present study, and dashed lines are calculations of Selleby and Sundman.[2] The step-like increase corresponds to incongruent melting.
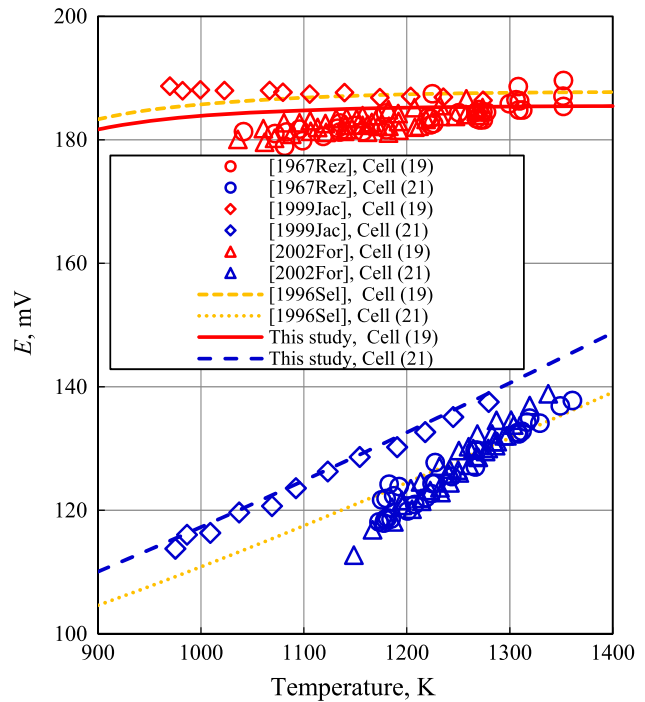

Fig. 7—EMF of the cells (19) and (21): experimental points[24–26] and calculated lines. Thick lines are calculations of the present study, and thin lines are calculations of Selleby and Sundman.[2]

For $Ca_2Fe_2O_5$ (C2F), the low temperature $C_P(T)$ was measured by King[21] from 53.3 K to 298.16 K (−219.7 °C to 25 °C) using adiabatic calorimetry. The entropy at 298.15 K (25 °C) was calculated to be $S^\circ_{298.15}$ = 188.7 ± 1.3 J mol⁻¹ K⁻¹. Rajagopalan et al.[22] used a laser flash method to measure the heat capacity of

Fig. 8—Normalized heat content of Ca$_2$Fe$_2$O$_5$: experimental points[23] and calculated lines. Solid lines are calculations of the present study, and dashed lines are calculations of Selleby and Sundman.[2] The step-like increase corresponds to congruent melting.
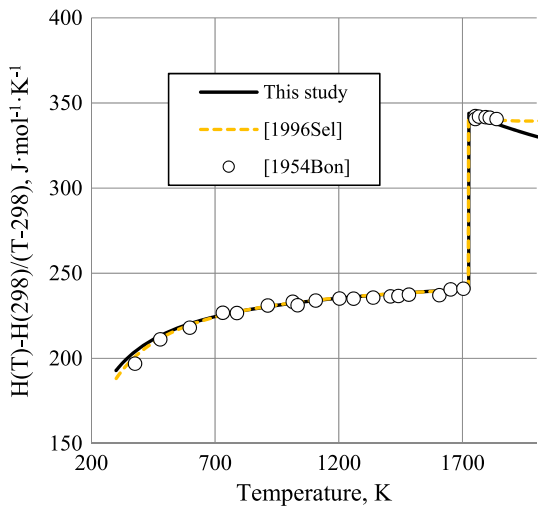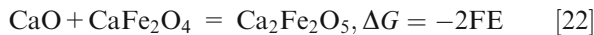
Ca$_2$Fe$_2$O$_5$ over the temperature range from 296 K to 1090 K (23 °C to 817 °C). The obtained results are in agreement with the sum of heat capacities of oxides and with the heat content data of Bonnickson,[23] who measured the heat content of C2F from 376.5 K to 1838 K (103.5 °C to 1565 °C). His data are shown in Figure 8.

Rezukhina and Bagin'ska,[24] Jacob et al.[25], and Forsberg et al.[26] measured the EMF of the following cell:

Pt, O$_2$, CaO + CaF$_2$|CaF$_2$|CaF$_2$ + CaFe$_2$O$_4$ + Ca$_2$Fe$_2$O$_5$, O$_2$, Pt   [21]
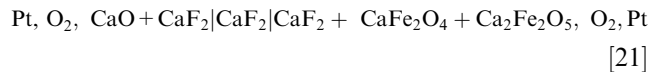
which corresponded to the Gibbs energy of the reaction.

$$CaO + CaFe_2O_4 = Ca_2Fe_2O_5, \Delta G = -2FE \quad [22]$$

The results are plotted in Figure 7. Again, there exists a discrepancy between Jacob et al.[25] and the other two studies.[24,26]

No heat capacity and entropy measurements are available for C4WF4, CWF, and CW3F.

Rosen and Saitton[4] and Li and Guo[5] determined the oxygen partial pressure for the CF + C2F + C4WF4 three-phase equilibrium using the EMF technique with calcia-stabilized zirconia as a solid electrolyte. In the former article,[4] pairs Ni-NiO or Cu-Cu$_2$O were employed as reference electrodes, while in the latter study,[5] the flow of air was used as a reference electrode. The results of Rosen and Saitton[4] and of Li and Guo[5] are plotted in Figure 9. There is a large discrepancy between two sets of data. The probable reasons are non-achievement of the target equilibrium and difficulty in maintaining inert condition of the cell. In a view of this discrepancy, the authors repeated the experiment of Rosen and Saitton.[4] The details are given in Aspiala et al.[6] and the results are plotted in Figure 9(b).

Reeve and Gregory[27] equilibrated mixtures of CaO and Fe$_2$O$_3$ with the flow of CO/CO$_2$ gas of controlled composition in Pt crucibles. After the equilibration, samples were quenched and analyzed for Fe^{2+}, Fe^{3+}, and Ca^{2+} using titration. Phases were identified by X-ray diffraction. The oxygen partial pressure over the Sp + C2F + CWF and Sp + Mono1 + CWF three-phase regions was determined as intermediate between two neighboring 2-phase regions. The experimental points are plotted in Figure 9. Reeve and Gregory[27] observed the C2F + CWF + Mono1. Later, it was confirmed by Bergman and Song[28] that CW3F is stable up to its melting point (see Section IV–G), and it is C2F + CW3F + Mono1 phase assemblage that should be stable at the temperatures of the experiment of Reeve and Gregory[27]. The reported oxygen potential over this three-phase region is shown in Figure 9.

Chung et al.[29] summarizes the results of previous measurements[30,31] on the reduction of calcium ferrite by the CO/CO$_2$ gas mixtures. The following EMF cell was used:

Pt, O$_2$, air or CO/CO$_2$|ZrO$_2$(Y$_2$O$_3$)|3 - phase mixture, Pt

[23]
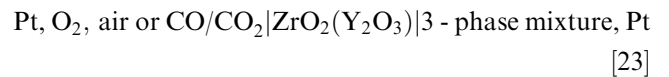
The reference electrode was either air or a CO/CO$_2$ mixture. When the CO/CO$_2$ mixture was used, its composition was adjusted until zero EMF was reached. The studied three-phase mixtures were Mono2 + C2F + Fe, Mono1 + C2F + Fe, CWF + C2F + CW3F, and Mono1 + C2F + CW3F. The results are given in Figure 9.

Tare and Deo[32] studied mixtures of lime and wüstite of several compositions using the EMF method with calcia-stabilized zirconia as a solid electrolyte and Fe/FeO reference electrode. At low temperatures, lime and wüstite reacted to form three-phase fields: either Mono1 + CF2 + Fe or Mono1 + CW3F + Fe. Bjorkman[33] used a similar method to study the equilibrium P(O$_2$) for three-phase equilibria Mono2 + C2F + Fe, Mono1 + Mono2 + Fe, Mono1 + C2F + Fe, and Mono1 + CW3F + Fe. The results are given in Figure 9. Two-phase equilibria Mono1 + Fe and Mono2 + Fe were also studied and are to be discussed in Section IV–C.

The experimental data of Burdese and Brisi,[34] Lykasov and Kozheurova,[35], Malquori and Cirilli[36], and Perrot[37] were assessed previously by Hillert et al.[1] They are plotted in Figure 9.

The experimental data on the oxygen potential for the three-phase equilibria fix the properties of CWF and CW3F rather well.

The properties of C4WF4 remain uncertain, even with the results of the recent experiments[4–6] (Figure 9(b)). According to the evaluation of Selleby and Sundman,[2] C4WF4 is rather stable and exists over a wide range of temperature and P(O$_2$). However, the calculated three-phase equilibrium Sp + CWF + C4WF4 is not in agreement with the observations of Reeve and Gregory,[27] who reports an Sp + C2F + CWF equilibrium instead at 1273 K (1000 °C) and oxygen potential −265 ± 3 kJ mol^{-1} (Figure 9(a)). There is also an
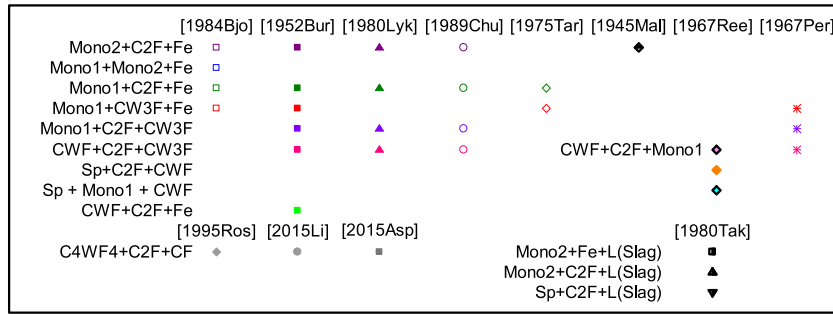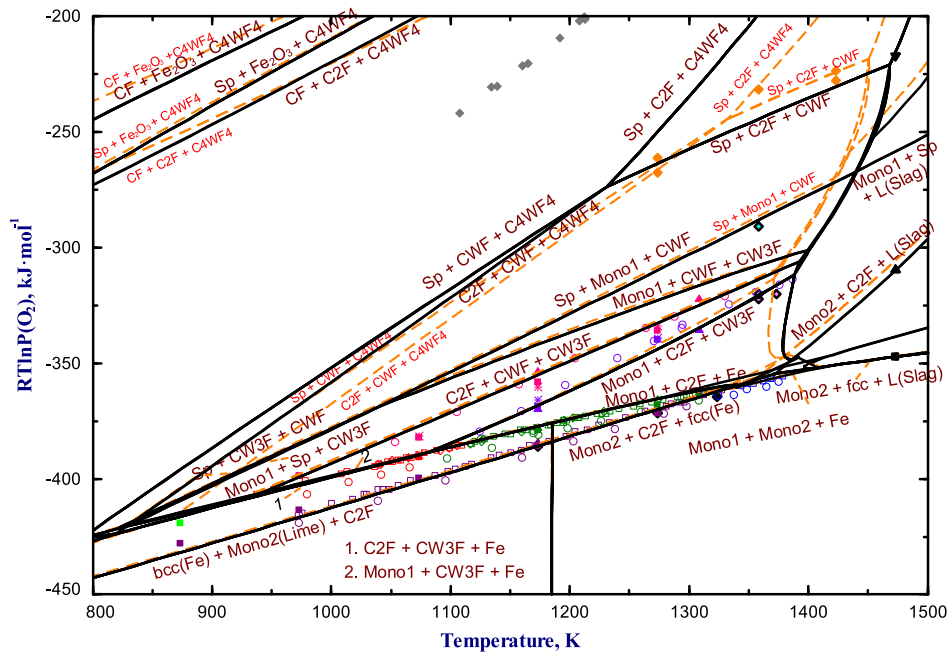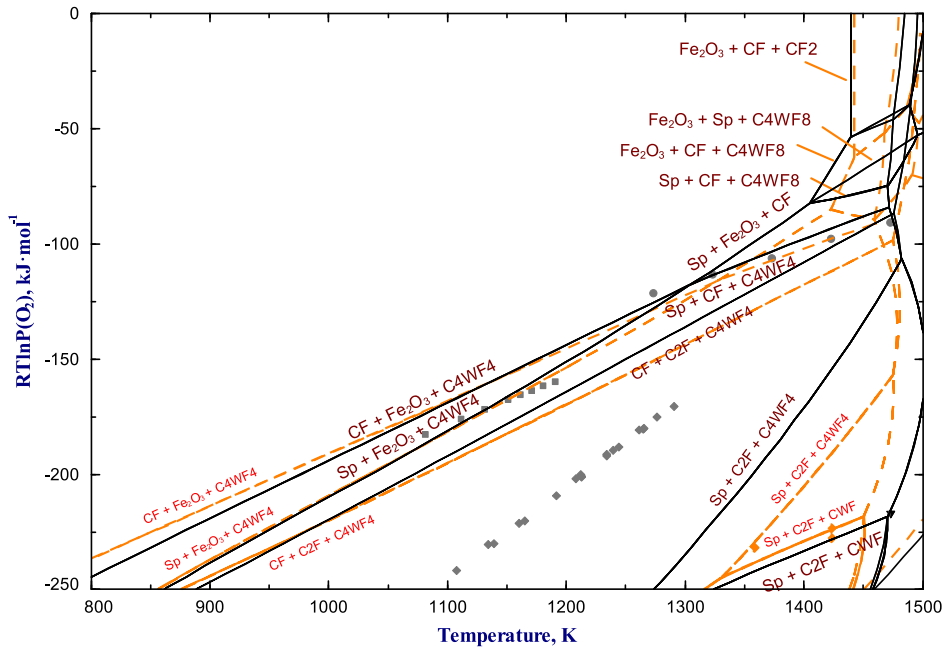
Fig. 9—Oxygen potential over three-phase regions in the Ca-Fe-O system: experimental points[4–6,27,29,32–37,39] and calculated lines are calculations of the present study, dashed lines are calculations of previous study,[2] and points are experimental data.

evidence of existence of C4WF4 phase in equilibrium with the Cu_2O-FeO-Fe_2O_3-CaO slag and liquid copper at 1373 K (1100 °C), as reported by Nikolic et al.[38] This fact will be used in the present study.

Very little information is available for the other two ternary compounds, $CaFe_4O_7$ (CF2) and $Ca_4Fe_{17}O_{29}$ (C4WF8). The ranges of stability of CF2 and C4WF8 will be discussed in Section IV–B–3 and Section V, respectively.

B. Phase Diagrams

1. FeO-CaO in equilibrium with iron

There are numerous articles devoted to the experimental determination of the "FeO-CaO phase diagram at iron saturation." In order to proceed further, it is worth discussing different ways of representing the results of these experiments, since it is often a source of confusion in assessments of oxide systems. The portion of the phase diagram of the Ca-Fe-O system at 1473 K (1200 °C) is shown in Figure 10. It can be seen from the figure that the compositions of the Mono1 and liquid slag phases in equilibrium with iron are shifted from the FeO-CaO section towards higher oxygen content. In most experiments, the Ca/Fe ratio in these phases was measured, but the exact oxygen content was not.

To eliminate the uncertainty in the oxygen content, it is possible to project the compositions of these phases onto the FeO-CaO section through the oxygen corner as shown in Figure 10 by the magenta lines. This geometric operation preserves the metal ratio Ca/(Ca + Fe). For instance, if the EPMA technique is used, only the ratio of metals can be measured reliably. The precise measurements of the oxygen are very difficult due to the high absorption of its characteristic lines. Therefore, the projection through the oxygen corner is a reasonable choice to represent the results of EPMA studies. The same is true for wet chemical analytical techniques, in case when only total iron and total calcium contents are measured.

Only when special efforts are made to measure the Fe^{2+} and Fe^{3+} content of the phase after the equilibration, it is possible to represent the composition of the phase in the basis of FeO, Fe_2O_3, and CaO. In this case, the composition of the phase may be projected either through the oxygen corner or through the iron corner.

The latter operation is shown by the green lines in Figure 10. The reason why it is desirable sometimes to make the projection through the iron corner is that it corresponds to the standard calculation procedure of phase diagrams in software packages as FactSage or Thermocalc. The example of such diagram is shown in Figure 11 using black lines. The diagram in Figure 11 represents the FeO-CaO section of the ternary system, showing what phases are stable at a particular composition on the FeO-CaO join at a given temperature. At the same time, it shows the projection of the compositions of these phases at equilibrium onto the FeO-CaO section through the iron corner. Indeed, if one refers back to Figure 10 and trace the boundary between Mono1 + fcc(Fe) + L(Slag) and L(Slag) + fcc(Fe) phase fields, he will see that it connects the composition of the slag with almost pure iron, and the intersection with the FeO-CaO section gives the signal on the diagram in Figure 11. The results of the experiment, where phase boundaries are measured as functions of composition on the FeO-CaO section, can be compared with the projection through the iron corner. This statement is true for phase diagrams at metal saturation in other chemical systems, as soon as the metal of saturation does not dissolve much of the system components. The experimental techniques such as DTA and equilibration/quenching technique produce results which should be compared with projections through the iron corner if the overall composition is on the section. To prevent the confusion, calculations are made for both types of projections, through iron corner and through oxygen corner. They are shown in Figure 11.

Oelsen and Maetz[40] conducted the DTA of mixtures of wüstite and lime in iron crucible. The composition of wüstite is not provided by the authors as well as procedure to recalculate the compositions to FeO-CaO section. Presumably, the correction on the non-stoichiometry of wüstite has been made. In this case, the position of the experimental points on the FeO-CaO section corresponds to the projection through the iron corner (Figure 11).

Abbattista et al.[41] prepared samples from $CaCO_3$, Fe_2O_3, and excess Fe. Samples were equilibrated in Pt crucibles under the flow of helium at temperatures 1123 K to 1403 K (850 °C to 1130 °C). After the equilibration, they were quenched in water with ice,
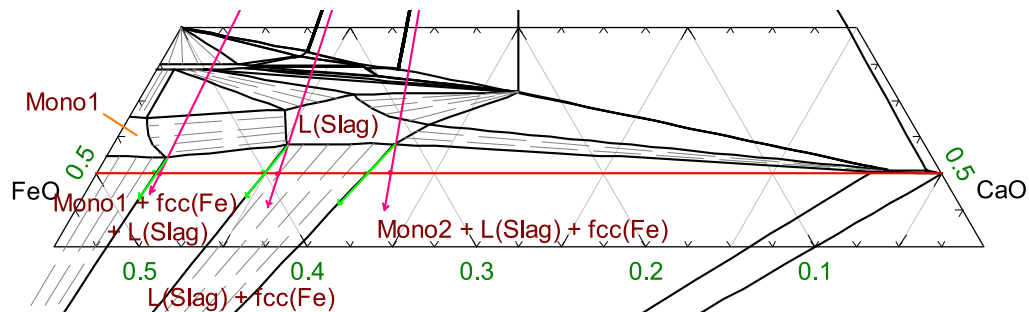

Fig. 10—Magnification of the phase diagram of the Ca-Fe-O system at 1473 K (1200 °C) showing two types of projection: the projection through the iron corner is shown by the green lines and the projection through the oxygen corner is shown by the magenta lines.
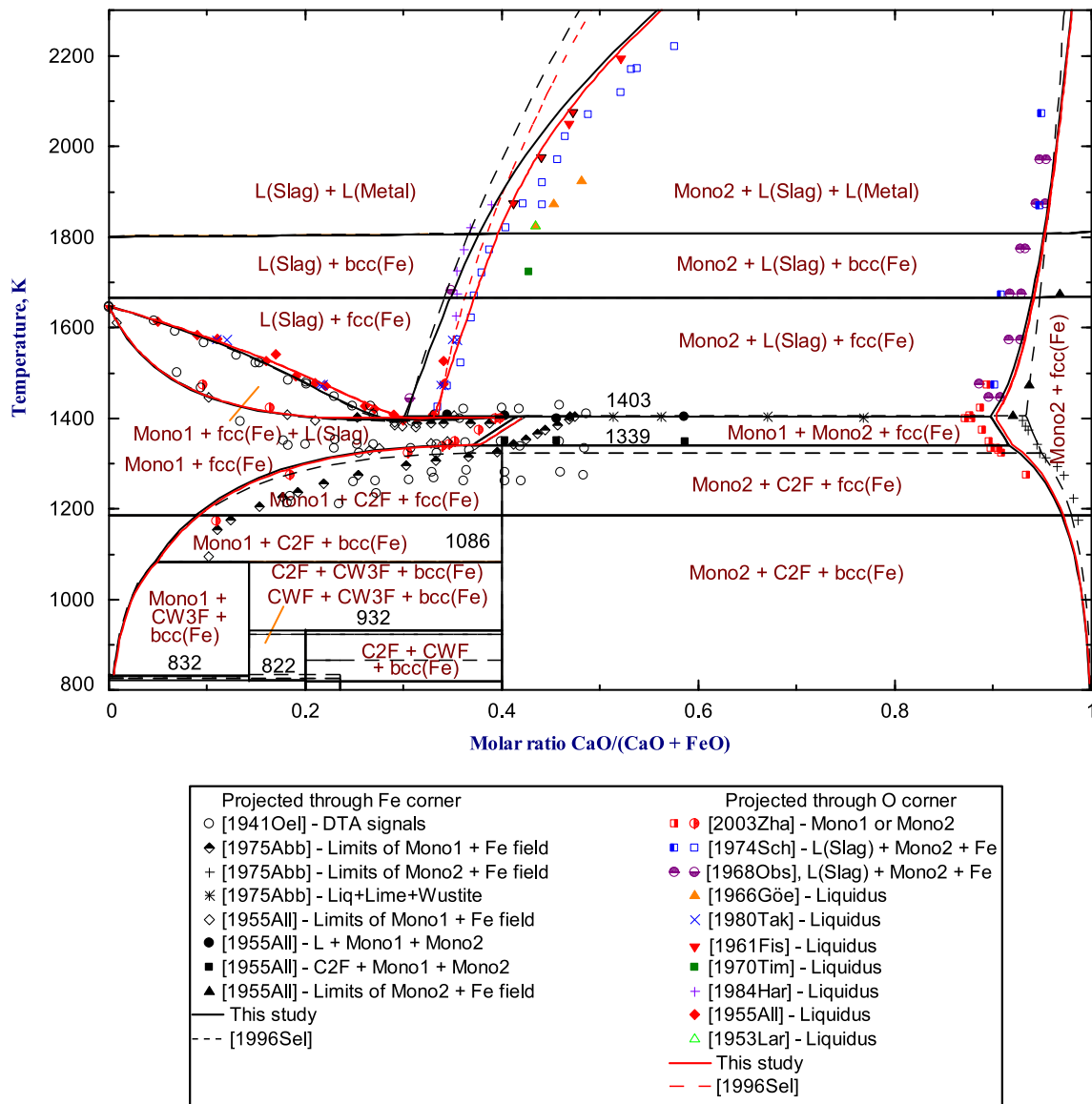
Fig. 11—FeO-CaO section of the Ca-Fe-O phase diagram: experimental points[39–50] and calculated lines. The calculations of the present study are shown by the solid lines, and the calculations of Selleby and Sundman[2] are shown by the dashed lines. Black lines show phase boundaries; red lines show the calculated compositions of the liquid slag, Mono1 and Mono2 phases projected to the FeO-CaO section through the oxygen corner.

and studied by XRD. The authors observed phase transitions at 1318 ± 5 K (1042 °C) and at 1403 ± 5 K (1130 °C), which corresponded to the decomposition of C2F and to the formation of liquid, respectively. The compositions of Mono1 and Mono2 were determined from XRD using the Vegard's law. They are plotted in Figure 11 and correspond to the projection through the iron corner.

Zhao et al.[42] equilibrated samples of lime and wüstite in iron crucibles under the flow of argon at 1173 K to 1473 K (900 °C to 1200 °C). After the equilibration, samples were quenched and analyzed using EPMA equipped with WDS detector. The resulting points are plotted in Figure 11. They were projected through the oxygen corner.

Larson and Chipman[43] equilibrated the slag samples with air or CO/CO_2 mixtures in Pt crucibles at 1823 K (1550 °C). After the equilibration, samples were quenched in liquid mercury and analyzed for total Fe, Fe^{2+}, and Fe^{3+}. The content of CaO was determined by difference. The break in the $Fe^{3+}/(Fe^{3+} + Fe^{2+})$ vs $CaO/(CaO + FeO + Fe_2O_3)$ line for a given $P(O_2)$ indicated the saturation with the solid phase. A single experimental point corresponding to saturation with iron and lime was projected through the oxygen corner and shown in Figure 11. The Fe^{3+} content in this point is plotted in Figure 12.

Allen and Snow[44] prepared the samples from ferrous oxalate and calcium carbonate. The mixtures were equilibrated in iron crucibles under N_2 atmosphere.
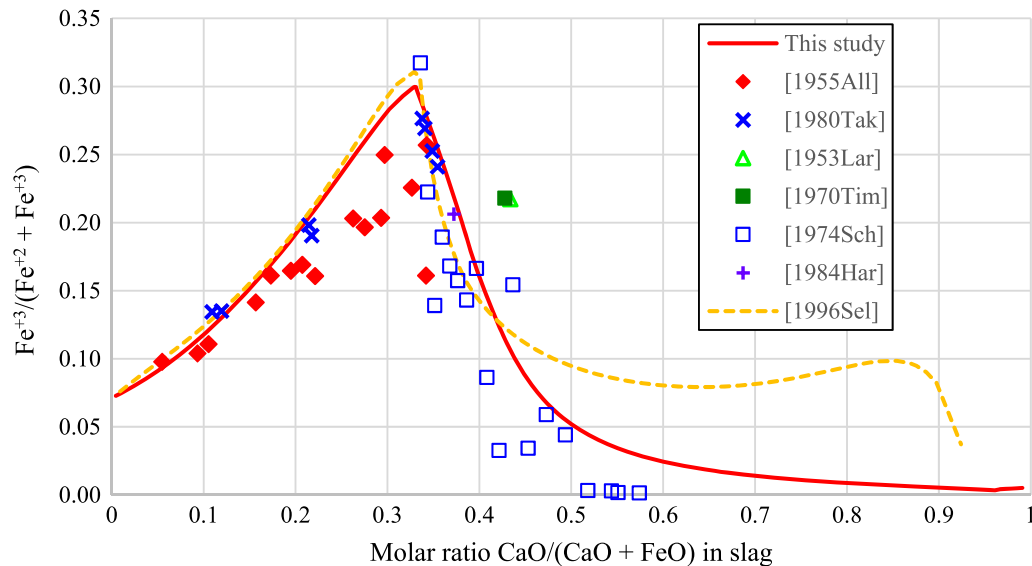
Fig. 12—The Fe^{3+} content in slag saturated with iron and solid oxide phases at liquidus temperatures: experimental points[39,43,44,48–50] and calculated lines. The calculations of this study are shown with a solid line, and the calculations of Selleby and Sundman[2] are shown with a dashed line. X-axis represents the projection of the liquid slag composition onto the FeO-CaO section through the oxygen corner.

After the equilibration, the samples were quenched in a water-isopropanol solution. The first portion of samples was analyzed for phase composition by optical microscopy and XRD. These results are shown with black symbols. The second portion of samples was re-equilibrated in a crucible at temperature, closer to the liquidus. After quenching and crushing, free iron particles were removed with a magnet. The remaining quenched liquid was analyzed for total iron and Fe^{2+} and CaO by wet chemical methods. The composition is represented in the basis of (FeO, Fe_2O_3, CaO). The projection of the liquid slag composition through the oxygen corner is plotted in Figure 11 using red symbols. The measured Fe^{3+} content as a function of slag composition at liquidus temperatures is shown in Figure 12.

Fisher and Fleischer[45] equilibrated FeO-CaO-MnO slag and liquid iron samples in lime crucible in air. Since the amount of liquid iron was large, around 500 g, it was not oxidized during the experiment. However, the fact that the reducing atmosphere was not created adds uncertainty on whether the equilibrium between slag, liquid iron, and lime was really established. After the equilibration, samples of iron and slag were taken with a quartz tube. The slag was analyzed for total iron, manganese, and calcium. The extrapolation of the compositions to manganese-free slag, projected through the oxygen corner, is plotted in Figure 11. The Fe^{3+} content at this point is plotted in Figure 12.

Görl et al.[46] equilibrated the mixtures of CaO-FeO-SiO_2 slags and iron and small quantities of sulfur in lime crucibles at 1823 K, 1873 K, and 1923 K (1550 °C, 1600 °C, and 1650 °C). The quenched slags were analyzed for total iron, Fe^{3+}, silica, and sulfur. The sulfur content was always <1 wt pct. For low-SiO_2 slag, the Fe^{3+} content was not measured. Figure 11 shows the extrapolation of slag compositions to the SiO_2-free system. They were projected through the oxygen corner.

Takeda et al.[39] equilibrated the mixtures of CaO, Fe_2O_3, and Fe in iron or Pt crucibles under a controlled atmosphere of CO/CO_2 at 1473 K and 1573 K (1200 °C and 1300 °C). After the equilibration, samples were quenched and crushed. Iron particles were removed with a magnet. The top and bottom parts of the samples were analyzed individually for total iron, Fe^{3+}, and Ca^{2+}. The difference in the measured metal contents between the top part, the bottom part, and the original charge indicated the precipitation of the solid phase. The exact composition of liquid in equilibrium with solid was obtained by extrapolating the compositional difference towards zero. The compositions of liquid in saturation with iron and either wüstite or lime are shown in Figure 11. The experimental points were projected through the oxygen corner. The ferrous/ferric ratio in this liquid is plotted in Figure 12.

Obst et al.[47] conducted an EPMA study of CaO-FeO slags in saturation with iron and lime. Samples were equilibrated in iron crucibles below 1723 K (1450 °C) or in lime crucibles above 1723 K (1450 °C). In the latter case, an excess iron was added. The quenched samples were analyzed by optical microscopy and EPMA with WDS detector. Thus, metal ratio in slag and Mono2 phases was obtained. The experimental points are plotted in Figure 11. They correspond to the projections of liquid and Mono2 compositions projected through the oxygen corner.

Timucin and Morris[48] conducted an experiment similar to Larson and Chipman.[43] The slags were prepared from $CaCO_3$ and Fe_2O_3 and equilibrated with the flow of CO/CO_2 or O_2/N_2 gas in Pt or Pt-Rh crucibles at 1723 K and 1823 K (1450 °C and 1550 °C). After the equilibration, samples were quenched in isopropyl alcohol and studied by optical microscopy. Optical microscopy showed whether the sample composition lays in the single-phase region or liquid + solid region. A single-phase liquid was analyzed for Fe^{2+},

total iron, and Ca^{2+}. At 1723 K (1450 °C), experiment with iron crucible was conducted to determine the position of double saturation with iron and Mono2. The composition of liquid at double saturation, projected through the oxygen corner, is shown in Figure 11. The Fe^{3+} content at this point is plotted in Figure 12.

Hara et al.[49] equilibrated mixtures of hematite and iron in lime crucibles for 4 hours at temperatures from 1623 K to 1873 K (from 1350 °C to 1600 °C). Quenched samples were analyzed by EPMA with the EDS detector. There may be uncertainty in the data since EDS detector is known only suitable for qualitative measurement. Results are shown in Figure 11. The points were projected through the oxygen corner. In another series of experiments, a mixture of hematite and lime was equilibrated under the flow of CO_2/H_2 in Pt-Rh crucibles. The oxidation state of iron was determined from the weight loss measured by a thermobalance. The Fe^{3+} content of slag, saturated with lime and iron, is obtained by the extrapolation and plotted in Figure 12.

Scheel[50] heated the FeO and CaO in lime crucibles. Three different gas mixtures were used: the flow of unspecified neutral gas, the CO/CO_2 mixture with $P(O_2) = 10^{-5}$, and the flow of air. In the first case, an excess of metallic iron was added to the crucible. After the equilibration, samples were quenched, and the slag and lime (Mono2) phases were separated using the undisclosed method. It is not reported how the excess iron was eliminated from the slag. The slag was analyzed chemically for total iron, Fe^{3+}, and Ca^{2+}, and the Mono2 phase was analyzed for total iron. Selected samples were studied using the EPMA. The type of detector is not reported. The results for neutral gas and iron saturation are plotted in Figures 11 and 12. The results for $P(O_2) = 0.21$ atm are discussed in Section IV–B–3. The results for $P(O_2) = 10^{-5}$ atm were taken into account in the assessment, but they are not plotted.

The comparison of experimental data in Figure 11 shows that there is a significant discrepancy in the composition of liquid slag and Mono2 (lime), particularly for L(Slag) + Mono2 + Fe equilibrium.

2. Isothermal Sections

Figures 13 through 19 show the CaO-FeO-Fe_2O_3 portions of the isothermal sections of the Ca-Fe-O phase diagram at temperatures 1473 to 1873 K (1200 °C to 1600 °C). Along with the phase boundaries, the oxygen isobars are calculated and compared with the available experimental data.

The experiments of Takeda et al.[39] (Figures 13, 14), Larson and Chipman[43] (Figure 18), Timucin and Morris[48] (Figures 16, 18), and Hara et al.[49] (Figure 17) were described earlier in Section IV–B–1.
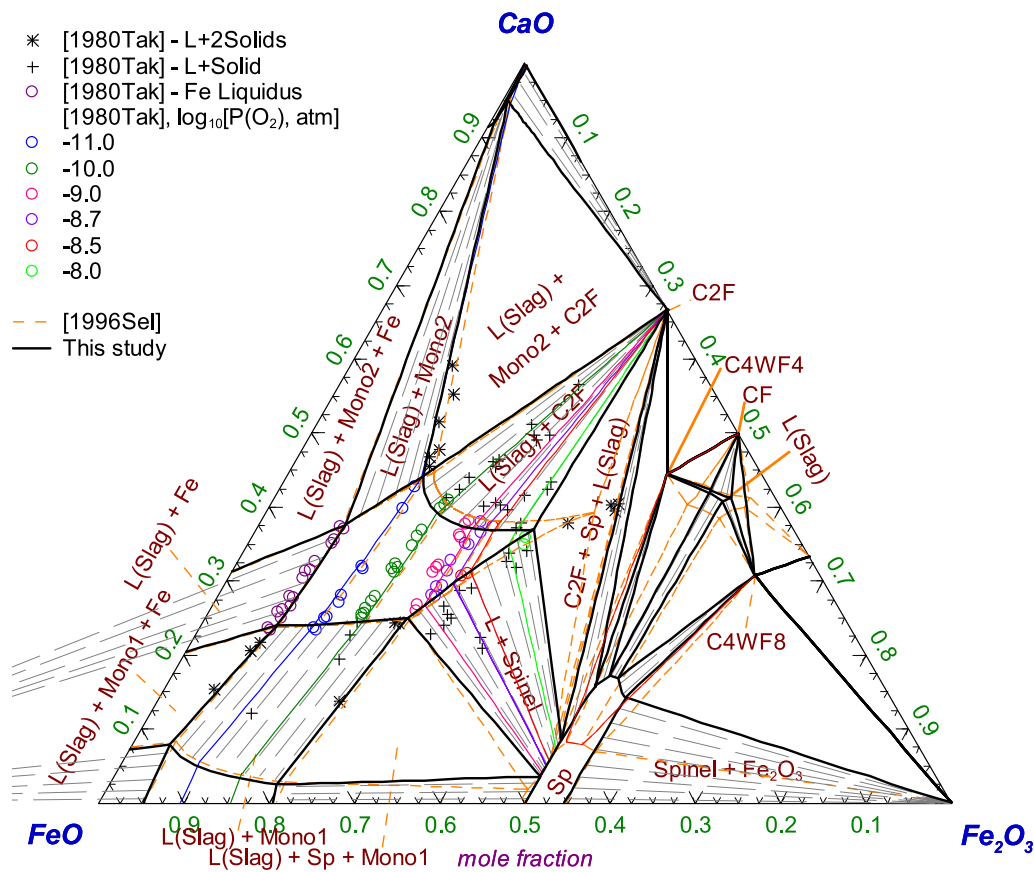

Fig. 13—The CaO-FeO-Fe₂O₃ portion of the isothermal section of the Ca-Fe-O phase diagram at 1473 K (1200 °C) and total pressure 1 atm: experimental points[39] and calculated lines. The calculations of the present study are shown by the solid lines, and the calculations of Selleby and Sundman[2] are shown by the dashed lines.

Fig. 14—The CaO-FeO-Fe$_2$O$_3$ portion of the isothermal section of the Ca-Fe-O phase diagram at 1573 K (1300 °C) and total pressure 1 atm: experimental points[39] and calculated lines. The calculations of the present study are shown by the solid lines, and the calculations of Selleby and Sundman[2] are shown by the dashed lines.
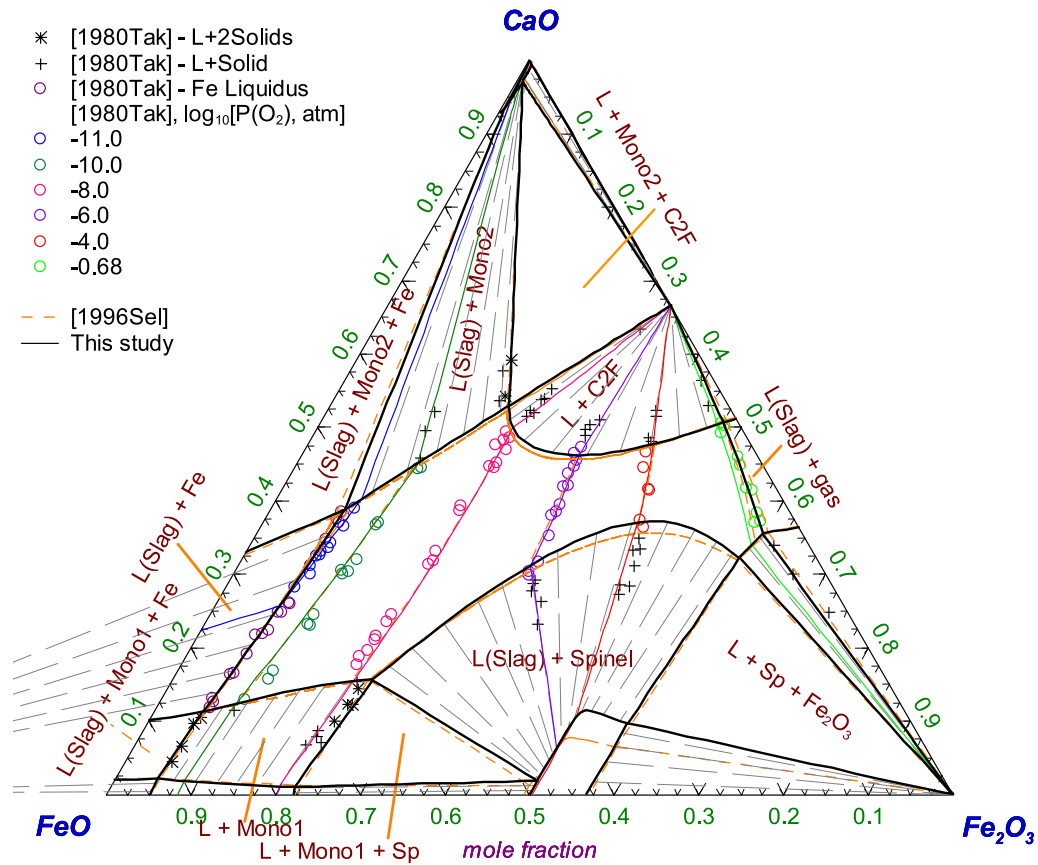
Ban-Ya *et al.*[51] equilibrated slags with the H$_2$O/H$_2$ gas mixture in iron crucibles. After the equilibration, samples were quenched, and the slag was separated and analyzed for total iron, Fe^{2+}, and Ca^{2+}. The composition of slag is plotted in Figure 15.

White[52] measured the composition of slag in equilibrium with N$_2$/O$_2$ gas mixtures in Pt crucible. A high-temperature balance was used to measure the loss of oxygen from the initial Fe$_2$O$_3$-CaO mixture, which gave the number of moles of FeO. The results are plotted in Figures 15 and 19.

Gurry and Darken[53] equilibrated mixtures of Fe$_2$O$_3$ and CaO with O$_2$ gas or CO$_2$ gas in Pt crucibles. The quenched samples were analyzed for total iron, Fe^{2+}, and Ca^{2+}. The composition of slag is plotted in Figure 19.

It is not possible to directly compare the results of different authors. They obtained the isobars for different partial pressures of oxygen and at different temperatures. The indirect comparison is possible using thermodynamic calculations.

3. *Fe$_2$O$_3$-CaO at High P(O$_2$)*

Figures 20 and 21 show the phase diagrams at fixed oxygen partial pressures, 0.21 and 1 atm, respectively. When the oxygen partial pressure is fixed, the projections of phase compositions through the oxygen corner onto a given section coincide with the phase boundaries on this section. Only the metal ratio in the bulk composition is important. This means that it is easier to interpret the experimental results and compare them with calculations than it was in the case of phase the diagrams at metal saturation. It is only necessary to choose a section on which the phase compositions will be projected. It is possible to use the Fe$_2$O$_3$-CaO section, the FeO-CaO section, or even the Fe-Ca section. Traditionally, for the phase diagrams at P(O$_2$) = 0.21 and 1 atm, the Fe$_2$O$_3$-CaO section is selected. The choice of the Fe$_2$O$_3$-CaO section does not mean that the equilibrium amounts of FeO in the phases under these conditions are negligible. The oxygen isobars in Figures 14 through 19 show that the slag contains a substantial amount of FeO even at high P(O$_2$).

Phillips and Muan[54] melted the mixtures of Fe$_2$O$_3$ and CaO in Pt crucibles in air or in oxygen at several temperatures. The samples were quenched and studied by XRD and optical microscopy. In some cases, when it was hard to distinguish the quenched crystals from primary crystals, high-temperature XRD was used. A portion of the quenched samples was crushed and analyzed for Fe^{2+}. The total iron content was determined only for several samples to confirm that it
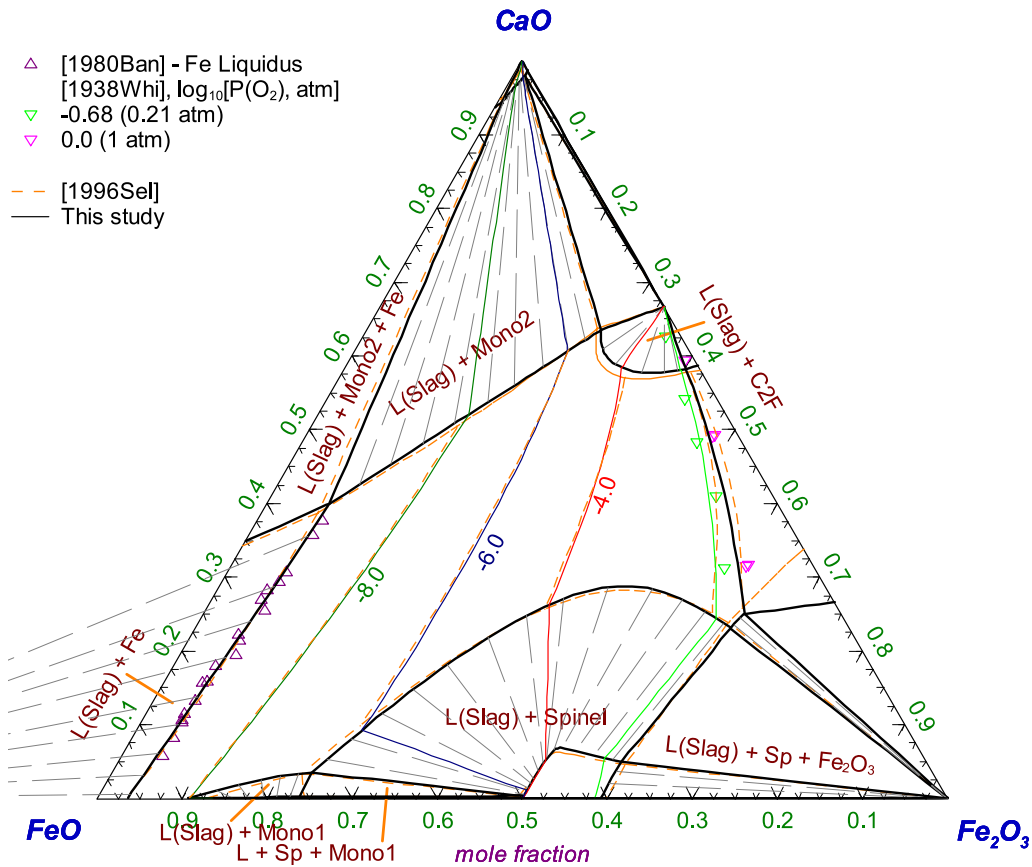
Fig. 15—The CaO-FeO-Fe$_2$O$_3$ portion of the isothermal section of the Ca-Fe-O phase diagram at 1673 K (1400 °C) and total pressure 1 atm: experimental points[51,52] and calculated lines. The calculations of the present study are shown by the solid lines, and the calculations of Selleby and Sundman[2] are shown by the dashed lines.

corresponded to the initial amount of Fe$_2$O$_3$. Based on the quenching experiments, Phillips and Muan[54] suggested the phase boundaries which are plotted in Figures 20 and 21.

The experiments of Scheel[50] were described earlier. The data points corresponding to $P(O_2)$ = 0.21 atm are plotted in Figure 20. It should be noted that the original diagram presented by Scheel[50] is contradictory. The X-axis is reported to be the mass ratio CaO/(CaO + FeO$_n$), but the composition of the C2F phase is plotted at 0.41, which is consistent with the projection onto the CaO-Fe$_2$O$_3$ section and X-axis being the mass ratio CaO/(CaO + Fe$_2$O$_3$). This letter interpretation was adopted in the present study and was used to plot the experimental results.

Hara *et al.*[49] equilibrated mixtures of hematite in lime crucibles for 4 hours at temperatures from 1623 K to 1873 K (1350 °C to 1600 °C). The quenched samples were analyzed by EPMA with an EDS detector. The results are shown in Figure 20.

The experiments of Timucin and Morris[48] were described earlier in Section IV–B–1. The optical microscopy observations of the quenched samples indicated the position of the Mono2 liquidus as shown in Figure 21.

Phase relations involving the CF2 phase are the only source of data available to fix its thermodynamic

properties. Phillips and Muan[54] suggested that it is stable between 1428 K and 1499 K (1155 °C and 1226 °C) in air and between 1445 K and 1501 K (1172 °C and 1228 °C) at $P(O_2)$ = 1 atm. Edsröm[55] studied the stability region of CF2 at $P(O_2)$ = 1 atm by a sintering/quenching/XRD method and found it to be 1393 K to 1501 K (1120 °C to 1228 °C). Phillips and Muan[54] cited the results of Batti,[56] who suggested the stability range of CF2 in air to be 1403 K to 1503 K (1130 °C to 1230 °C). Liu[57] reports CF2 to be stable in air up to 1503 K (1203 °C). Although all the authors agree on the upper temperature of the stability region within 5 K (−268 °C), there is a large disagreement on the lower temperature. The decomposition of CF2 into Fe$_2$O$_3$ and CF is a sluggish solid-state reaction, which is difficult to study. In the present work, more weight was given to the results of Phillips and Muan,[54] who approached this reaction from both low- and high-temperature sides and equilibrated samples for up to 24 hours before quenching or used high-temperature XRD.

C. Monoxide

Tare and Deo[32] and Bjorkman[33] conducted an EMF study of mixtures of wüstite and lime. Both studies used calcia-stabilized zirconia as a solid electrolyte and a
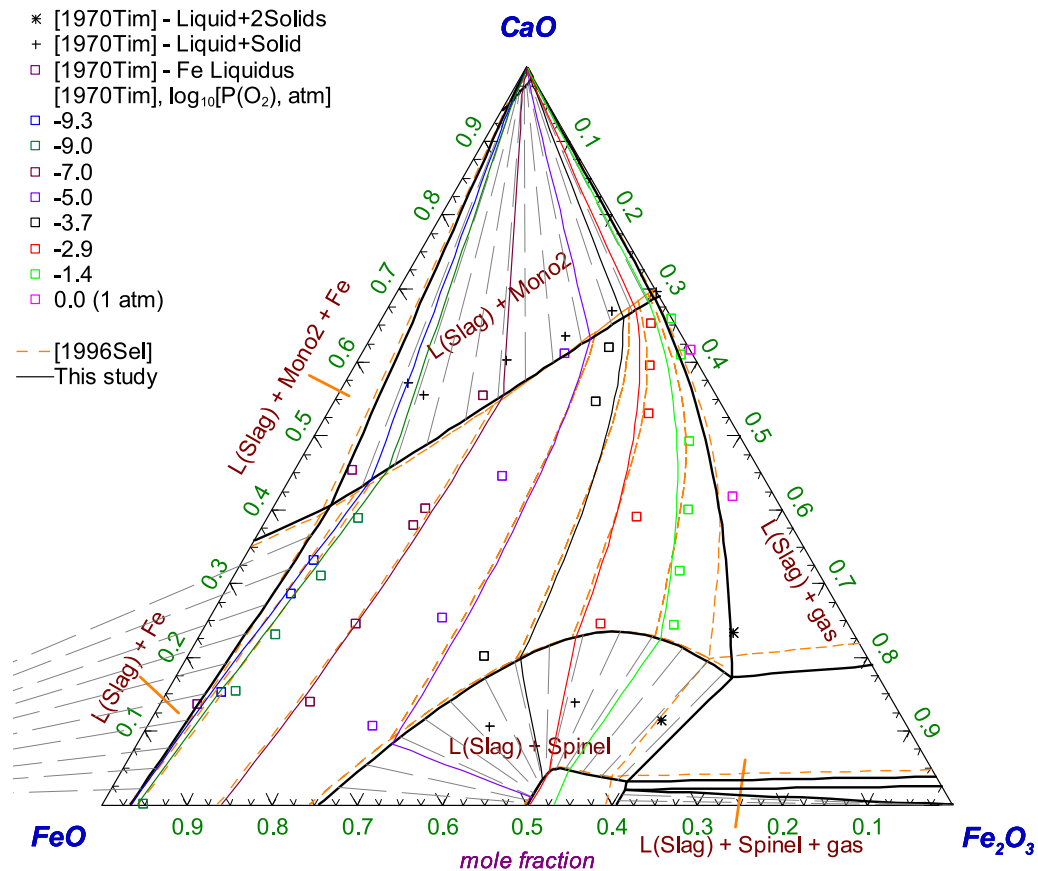
Fig. 16—The CaO-FeO-Fe$_2$O$_3$ portion of the isothermal section of the Ca-Fe-O phase diagram at 1723 K (1450 °C) and total pressure 1 atm: experimental points[48] and calculated lines. The calculations of the present study are shown by the solid lines, and the calculations of Selleby and Sundman[2] are shown by the dashed lines.

Fe/FeO reference electrode. Tare and Deo[32] reported the composition of wüstite to be FeO$_{1.06}$. Bjorkman[33] did not specify the composition of wüstite and reported the composition of the Mono1 phase in terms of "$X(Fe_tO)$". This representation is somewhat ambiguous and does not allow to establish the precise composition of the monoxide phase. However, the introduced uncertainty is small, less than 0.005 in molar ratio Ca/(Ca + Fe). In the present study, the EMF values at 1273 K, 1353 K, and 1373 K (1000 °C, 1080 °C, and 1100 °C) were obtained by linear regression of original data. They were recalculated to $P(O_2)$ and plotted in Figure 22.

Johnson and Muan[58] equilibrated mixtures of wüstite, lime, and silica in Pt crucibles with the flow of CO/CO$_2$ at 1353 K (1080 °C). After the equilibration, samples were quenched and analyzed by X-ray and optical microscopy. The CO/CO$_2$ ratio was varied until the precipitation of Fe was observed by optical microscopy. The bulk composition was located in the Mono2 + Ca$_2$SiO$_4$ + Fe and Mono1 + Ca$_2$SiO$_4$ + Fe regions. The oxygen partial pressure was calculated from the equilibrium CO/CO$_2$ ratio. In the present study, the reported activities were used to obtain $P(O_2)$ for the Fe + monoxide region. It is shown in Figure 22.

Abbattista et al.[41] reported the composition of CO/CO$_2$ mixtures in equilibrium with Mono1 + Fe. The

details of the experiment are not provided. The results are plotted in Figure 22.

D. Slag

The equilibrium partial pressure of oxygen for slags saturated with iron was studied by Takeda et al.[39], Ban-Ya et al.[51], and Iwase et al.[59]

The experiments of Takeda et al.[39] were described in Section IV–B–1, and the study of Ban-Ya et al.[51] was previously mentioned in Section IV–B–2. Their results are plotted in Figure 23.

Iwase et al.[59] measured the EMF of the galvanic cell:

$$Mo/Mo + MoO_2/ZrO_2(MgO) / Fe + FeO + CaO + Ag/Fe$$

[24]
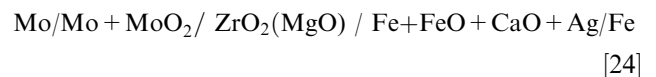
The measurements were performed at 1673 K (1400 °C). In the present study, the EMF values were recalculated to $P(O_2)$ using the first Ca-free point as a reference value. The results are shown in Figure 23.

Ban-Ya et al.[3] measured the heat of dissolution of solid CaO in liquid Fe-O slag placed in an iron crucible at 1693 K (1420 °C). The isoperibol calorimeter of the isothermal jacket type was used. After the heat effect was measured, the slag was quenched and analyzed for the total iron and calcium content. Unfortunately, the
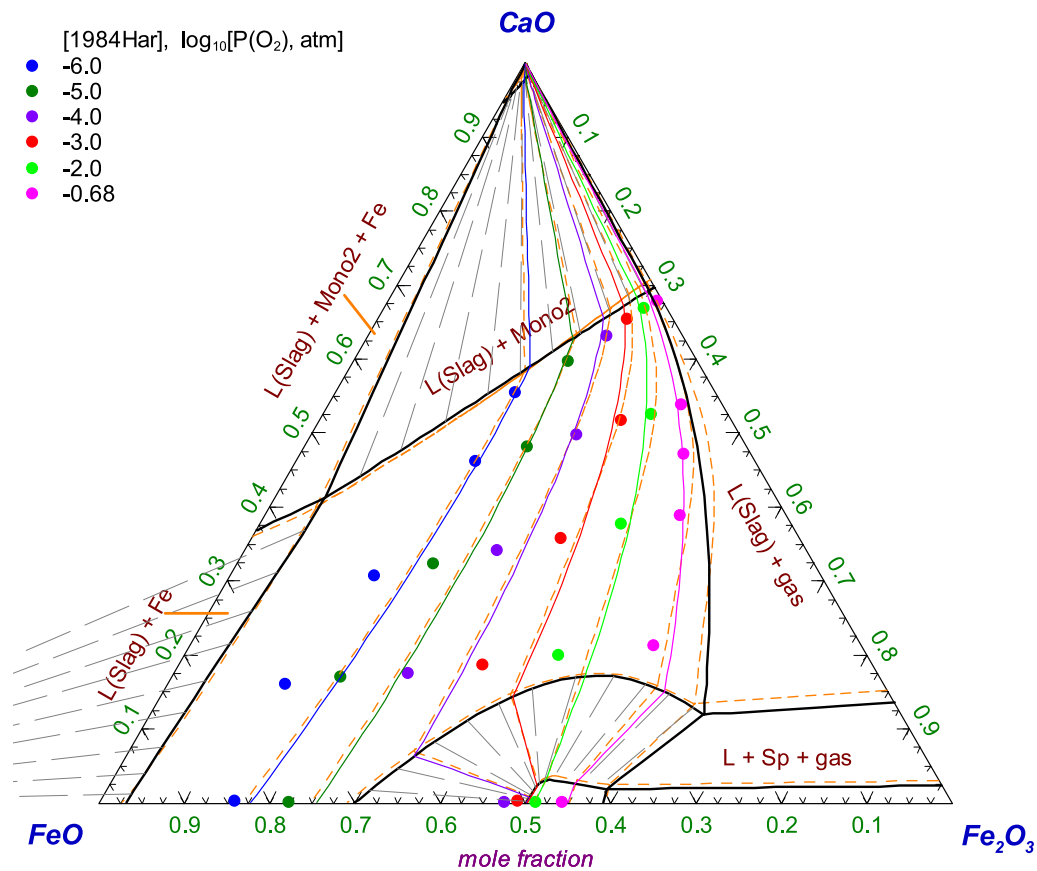
Fig. 17—The CaO-FeO-Fe$_2$O$_3$ portion of the isothermal section of the Ca-Fe-O phase diagram at 1773 K (1500 °C) and total pressure 1 atm: experimental points[49] and calculated lines. The calculations of the present study are shown by the solid lines, and the calculations of Selleby and Sundman[2] are shown by the dashed lines.

authors do not provide the primary data. Instead, they give the enthalpy of mixing between liquid Fe-O slag and liquid CaO. In order to obtain the latter values from the primary data, it is necessary to know the enthalpy of transition of solid CaO into liquid CaO at the temperature of the experiment [1693 K (1420 °C)]. The authors cited the work of Chang and Howald,[60] who gave the enthalpy of fusion as 59.05 kJ mol^{-1} at 3173 K (2900 °C) and gave the heat capacity functions of liquid and solid CaO. Based on the data of Chang and Howald,[60] the primary data of Ban-Ya et al.[3] were back-calculated in the present study (see Figure 24).

E. Solubility of Calcium in Spinel

Berggren[61,62] equilibrated small amounts of calcium oxalate with iron oxalate (or hydroxide) in Pt crucibles with a flow of CO/CO$_2$ gas for temperatures ranging between 1245 K and 1524 K (972 °C and 1251 °C). The Sp/Sp + CWF and Sp/Sp + slag phase boundaries were determined by selecting the oxygen partial pressure in such a way that the overall composition was located either in the single-phase region or in the corresponding two-phase region. The quenched samples were analyzed chemically for the overall CaO content and by XRD. The calcium content of spinel was obtained from the measured lattice parameters using the Vegards's law.

The experimental results are shown in Figure 25. As can be deduced from Figures 5 and 13, these points should be located below the Sp + C2F + CWF and above the Sp + CWF (or Slag) + Mono1 line in Figure 25.

Liu[57] used equilibration in Pt crucibles under the flow of Ar, followed by quenching and EPMA analysis. The experiments were conducted in the temperature range from 1323 K to 1473 K (1050 °C to 1200 °C), and the overall composition corresponded to the Sp + CF + C4WF4, Sp + C2F + C4WF4 or Sp + C2F + CWF field. The presence of the C4WF4 phase from 1323 K to 1473 K (1050 °C to 1200 °C) was confirmed. The measured calcium content is plotted in Figure 25.

F. Solubility of Oxygen in Liquid Metal

Ca behaves as an extremely strong deoxidant for steels. In the Ca-Fe-O system, the addition of small quantities of Ca to the Fe-O liquid metal causes, at first, formation of the slag phase (Figure 26). Adding more Ca results in precipitation of solid lime and a drop of oxygen content by several orders of magnitude. This effect was previously assessed by Jung et al.[63] The results of their evaluation along with the selected experimental data[64–69] are presented in Figure 27. Jung et al.[63] introduced CaO associates in the liquid metal phase in order to reproduce the experimental data. Even
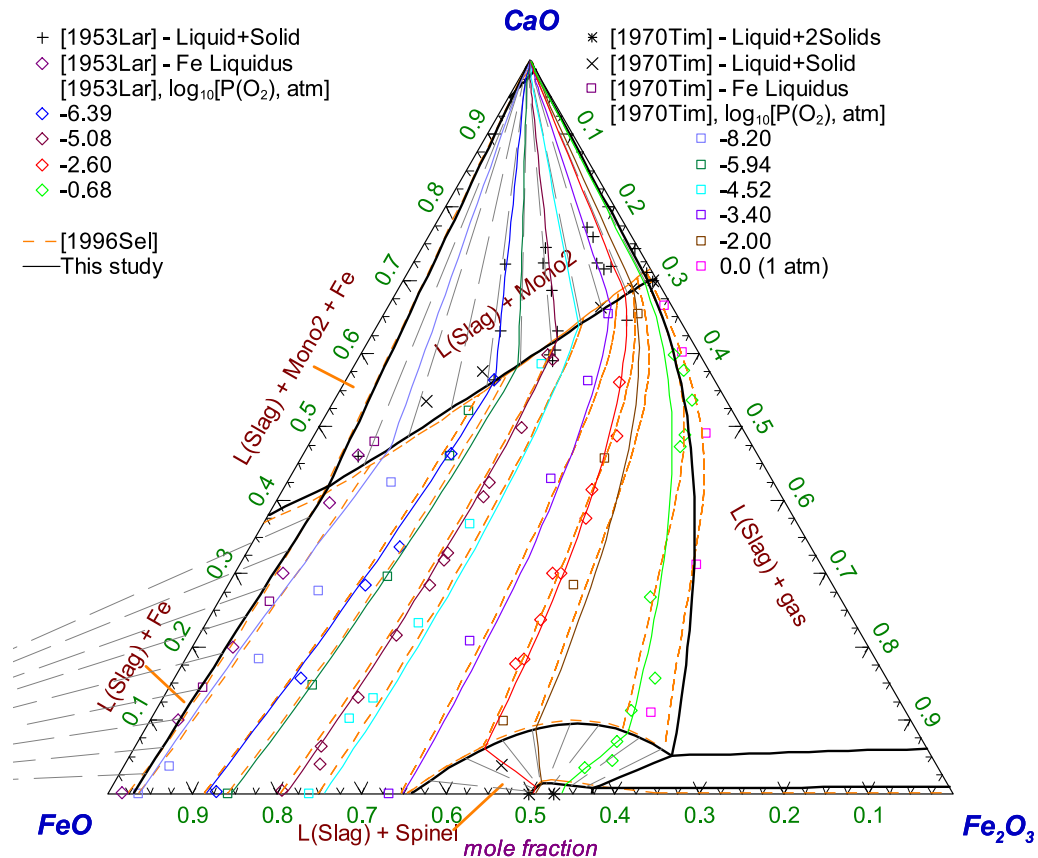
Fig. 18—The CaO-FeO-Fe₂O₃ portion of the isothermal section of the Ca-Fe-O phase diagram at 1823 K (1550 °C) and total pressure 1 atm: experimental points[43,48] and calculated lines. The calculations of the present study are shown by the solid lines, and the calculations of Selleby and Sundman[2] are shown by the dashed lines.

though the database of Selleby and Sundman[2] predicts the drop in the oxygen content with the addition of Ca to the liquid metal, it does not reproduce the experimental data quantitatively, as can be seen from Figure 27.

G. Liquidus Projection

The liquidus in the high-$P(O_2)$ region of the CaO-FeO-Fe₂O₃ phase diagram was studied by Phillips and Muan.[70] They used equilibration in sealed Pt-Rh crucibles followed by quenching and reflective optical microscopy analysis. Solid phases were identified by powder X-ray diffraction. Selected samples were analyzed chemically for the FeO content before and after the experiment to confirm that no change in the composition occurred. Based on the experimental results, the primary phase fields of spinel, Fe₂O₃, C2F, C4WF4, C4WF8, CF, and CF2 were constructed and invariant temperatures were suggested. These data are shown in Figure 28 and Table II.

The melting of CW3F phase was studied by Bergman and Song.[28] They sintered the mixture of CaO, Fe₂O₃, and Fe in sealed Pt crucible. The quenched samples were analyzed by the SEM. It was discovered that the CW3F phase does not decompose into solid phases before melting. The fine-structure regions were observed in

samples prepared at 1373 K (1100 °C). These regions were attributed to the formation of the liquid phase. The corresponding invariant points involving CW3F and liquid slag are shown in Table II.

V. OPTIMIZATION OF MODEL PARAMETERS

The optimization procedure was as follows. First of all, the heat capacity, entropy, and enthalpy of formation of CF and C2F were fixed using the data on heat content (Figures 6, 8), low temperature heat capacity data of King[21], and EMF data from Figure 7. In the latter case, more weight was given to the data of Jacob et al.[25]

The properties of wüstite-lime (monoxide) solid solution were established using the data in Figures 9a, 11, and 22. For the mutual solubility, the preference was given to the new data of Zhao et al.[42], which were obtained using the EPMA technique. Two excess parameters, $q^{11}_{CaO,FeO}$ and $q^{21}_{CaO,FeO}$, were optimized.

The heat capacities of CWF and CW3F were obtained by the increment method. The experimental data in Figure 9(a) were used to fix the entropy and enthalpy of formation of these compounds.

The solubility of Ca in spinel was established from the data in Figure 25. The enthalpy of formation and
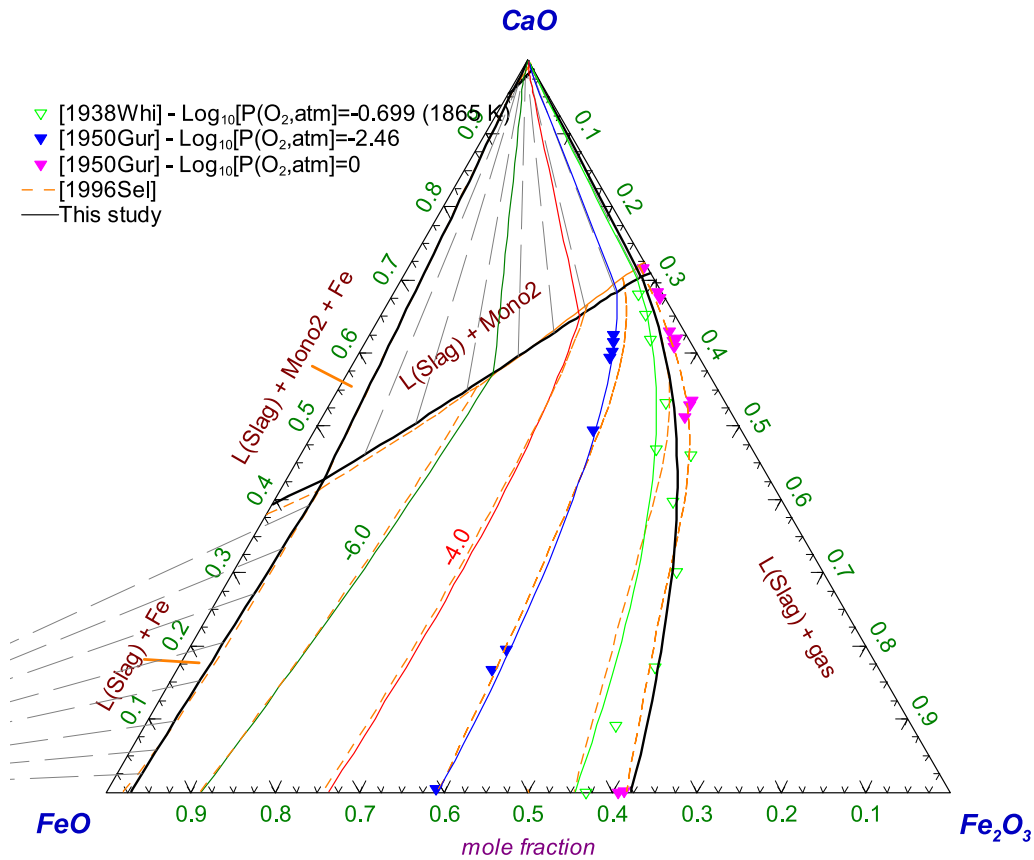
Fig. 19—The CaO-FeO-Fe₂O₃ portion of the isothermal section of the Ca-Fe-O phase diagram at 1873 K (1600 °C) and total pressure 1 atm: experimental points[52,53] and calculated lines. The calculations of the present study are shown by the solid lines, and the calculations of Selleby and Sundman[2] are shown by the dashed lines.
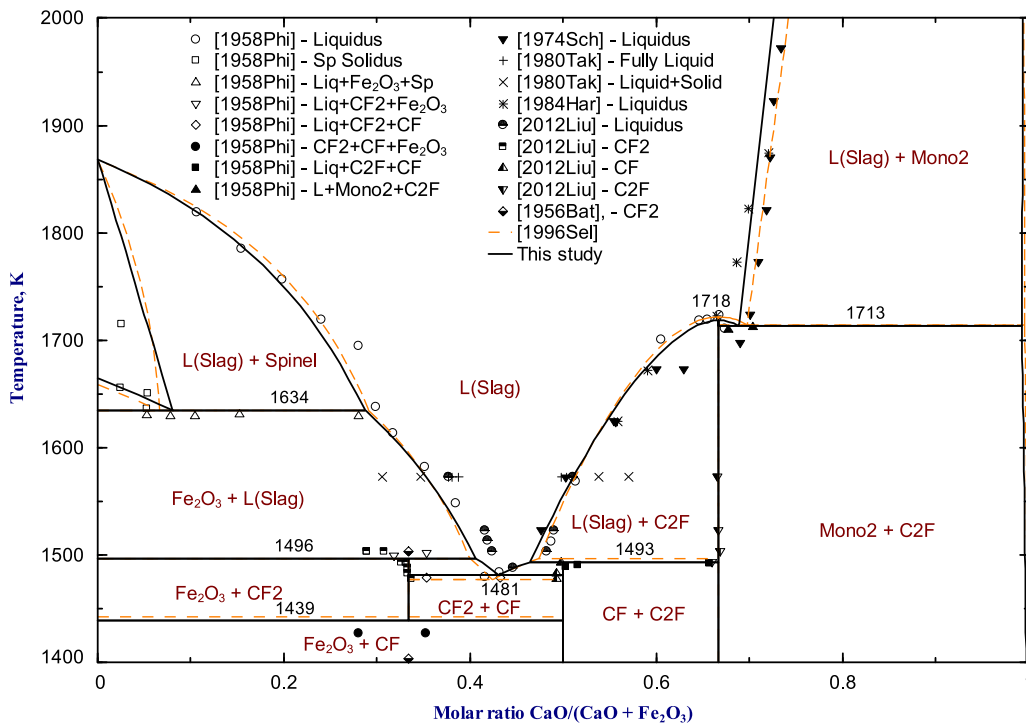

Fig. 20—The CaO-Fe₂O₃ section of the Ca-Fe-O phase diagram at $P(O_2) = 0.21$ atm: experimental points[49,50,54,56,57] and calculated lines. The calculations of the present study are shown by the solid lines, and the calculations of Selleby and Sundman[2] are shown by the dashed lines.

Fig. 21—The CaO-Fe$_2$O$_3$ section of the Ca-Fe-O phase diagram at $P(O_2) = 1$ atm: experimental points[48,54,55] and calculated lines. The calculations of the present study are shown by the solid lines, and the calculations of Selleby and Sundman[2] are shown by the dashed lines.

Fig. 22—Oxygen partial pressure for the Mono1 + Fe and Mono2 + Fe regions of the Ca-Fe-O system: experimental points[32,33,41,58] and calculated lines. The calculations of the present study are shown by the solid lines, and the calculations of Selleby and Sundman[2] are shown by the dashed lines.
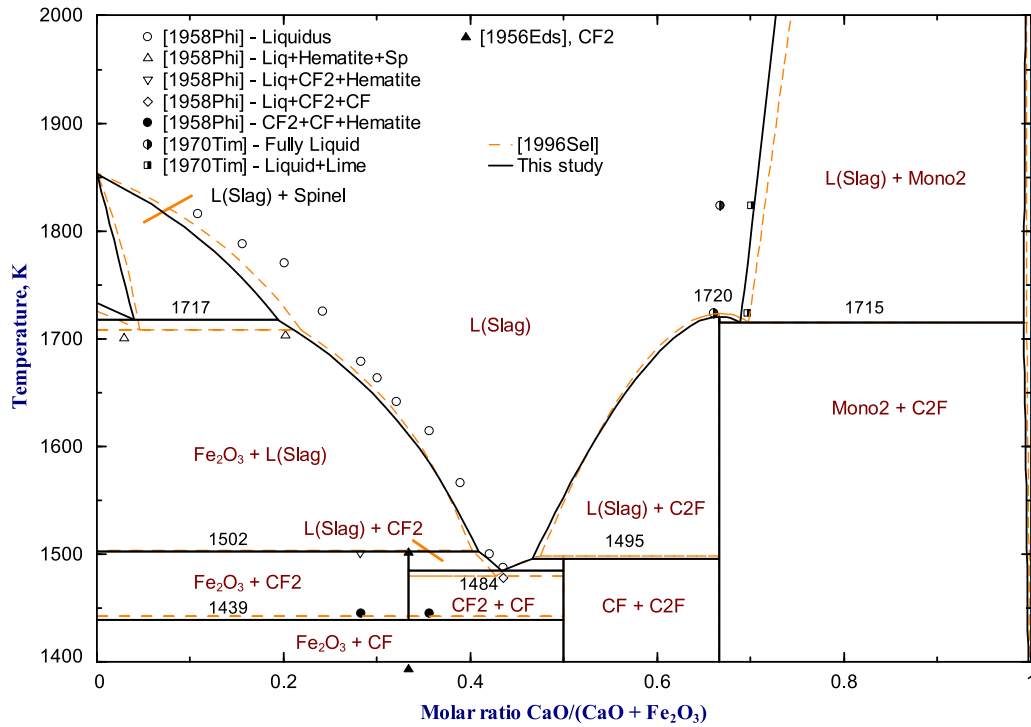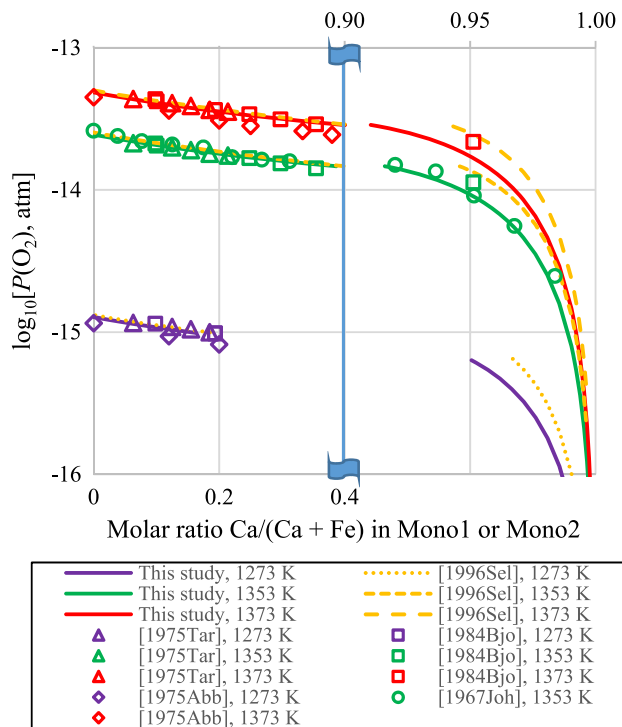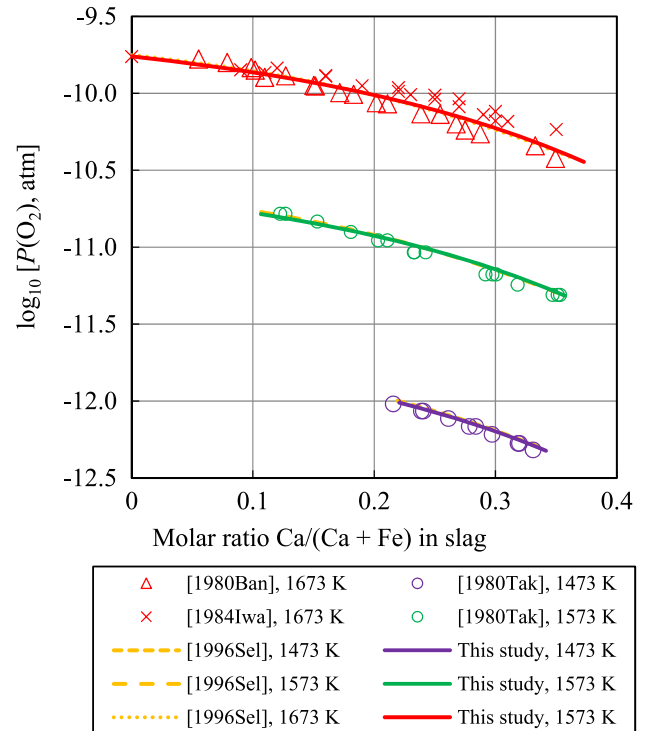

Fig. 23—Equilibrium oxygen partial pressure over L(slag) + iron: experimental points and calculated lines. Solid lines are the calculations of the present study, and dashed and dotted lines are the calculations of Selleby and Sundman.[2]
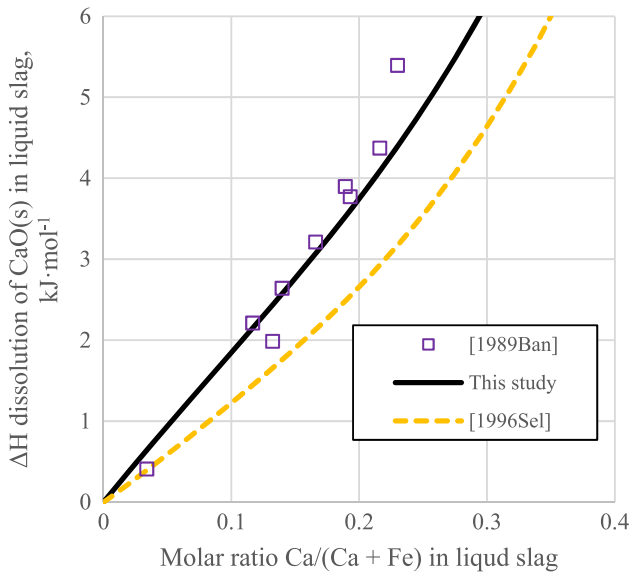
Fig. 24—Enthalpy of dissolution of solid CaO in liquid FeO slag in equilibrium with Fe at 1693 K (1420 °C): experimental points[3] and calculated lines. Solid line shows the calculations of the present study, and dashed line shows the calculations of Selleby and Sundman.[2]

entropy of the hypothetical neutral inverse spinel $(Fe^{3+})^{tetr}[Ca_{0.5}^{2+}, Fe_{0.5}^{3+}]_2^{oct}O_4^{-2}$ were optimized, while the heat capacity was assumed to be the same as for CaFe$_2$O$_4$. As can be seen from Figure 25, the optimized solubility of Ca in spinel is in agreement with the recent data of Liu[57] and the earlier data of Berggren[61,62] within the experimental accuracy. It is higher than obtained in the assessment of Selleby and Sundman.[2]

The heat capacity of C4WF4 was approximated by the increment method. The oxygen partial pressure over CF + C2F + C4WF4 data was used to set the enthalpy of formation and entropy. More weight was given to the data of Aspiala et al.[6] and Li and Guo[5] (Figure 9b). More positive enthalpy of formation could describe the data of Rosen and Saitton,[4] but as a result, C4WF4 would be unstable in equilibrium with the Cu$_2$O-FeO-Fe$_2$O$_3$-CaO slag and liquid copper at 1373 K (1100 °C), which contradicts the observations of Nikolic et al.[38] More negative enthalpy of formation compromises the Sp + CF + C4WF4 equilibrium at 1323 K (1050 °C) as reported by Liu[57] (Figure 25).

Optimizing the slag parameters was a challenge. The presence of iron in two oxidation states makes it necessary to adjust the FeO-CaO, Fe$_2$O$_3$-CaO, and CaO-FeO-Fe$_2$O$_3$ interactions simultaneously. However, the phase diagrams in air and in oxygen (Figures 20 and 21) are mostly defined by the Fe$_2$O$_3$-CaO parameters. Thus, in the first iteration, these phase diagrams were described using the $\Delta g_{Ca^{2+},Fe^{3+}}^{\circ}$, $g_{Ca^{2+},Fe^{3+}}^{01}$ and $g_{Ca^{2+},Fe^{3+}}^{10}$ parameters. The temperature dependence in $g_{Ca^{2+},Fe^{3+}}^{01}$ was necessary to describe the enthalpy of melting of CF and C2F (Figures 6, 8). Small adjustments in the entropy and enthalpy of formation of CF and C2F were made. Then, the $\Delta g_{Ca^{2+},Fe^{2+}}^{\circ}$ and $g_{Ca^{2+},Fe^{2+}}^{01}$ parameters were introduced to fit the phase diagram at iron saturation in
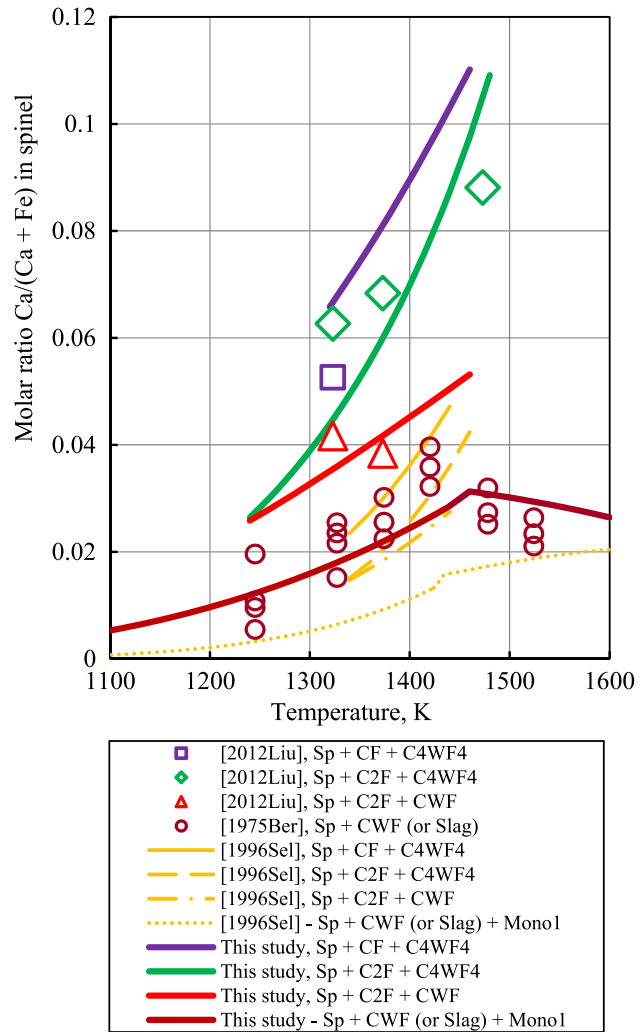

Fig. 25—Calcium content of spinel. Experimental points[57,62] and calculated lines. Thick lines are the calculations of the present study, and thin lines are the calculations of Selleby and Sundman.[2]

Figure 11. The resulting spinel and C2F liquid (Figures 13, 14) were too wide and the introduction of negative ternary parameters was necessary. After extensive trial and error attempts, parameters $q_{Fe^{3+},Ca^{2+}(Fe^{2+})}^{111}$ and $q_{Fe^{3+},Ca^{2+}(Fe^{2+})}^{011}$ were selected. They had effects on all the above-mentioned diagrams. Moreover, they had a major effect on the Fe^{3+} content of the iron-saturated slag (Figure 12). Because of the Toop-type extrapolation of the Fe$_2$O$_3$-CaO interactions into the ternary system, the curve in Figure 12 was also affected by the parameters on the Fe$_2$O$_3$-CaO side. The $g_{Ca^{2+},Fe^{3+}}^{20}$ parameter was introduced to achieve the drop in the Fe^{3+} content with the increase of the CaO content in accordance with the experimental data of Scheel.[48] The temperature dependence of $q_{Fe^{3+},Ca^{2+}(Fe^{2+})}^{111}$ and $q_{Fe^{3+},Ca^{2+}(Fe^{2+})}^{011}$ was necessary to describe Figure 12 and the enthalpy of dissolution of CaO in the iron-saturated slag (Figure 24). In the final cycle of optimization, all slag parameters were adjusted simultaneously to best describe all experimental data. The oxygen isobars in Figures 13 through 19 were taken into account.
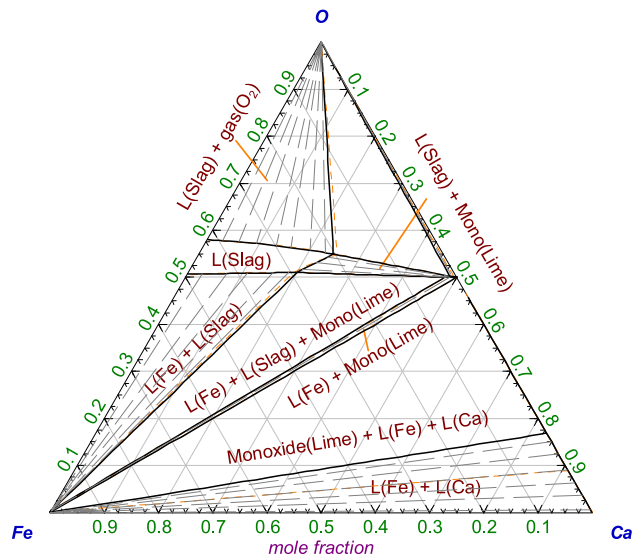
Fig. 26—Phase diagram of the Ca-Fe-O system at 1873 K (1600 °C). Thick lines are calculated in the present study, and thin lines are calculated using the database from.[2] The formation of the gaseous Ca is suppressed.

The heat capacity of the CF2 and C4WF8 phases were approximated by the increment method. For CF2, the enthalpy of formation and entropy were fixed using the range of stability in air and in oxygen (Figures 20, 21). For C4WF8, the enthalpy and entropy were chosen in such a way that stability range of CF2 and C4WF8 was similar to that predicted by Selleby and Sundman[2] (Figure 9; Table II).

For the liquid metal phase, the $L^0_{Ca,CaO}$ parameter was introduced to describe Figure 2. All other parameters were taken from Jung et al.[63]

All the calculations in Figures 1 through 28 were made using the final set of model parameters. The list of parameters is given in Table III. The results are compared with experimental data and with the previous thermodynamic optimization of Selleby and Sundman.[2]

Fig. 27—Oxygen content of Fe-Ca alloys, coexisting with oxide phases at 1873 K (1600 °C). Solid lines are calculations of the present study, and dashed lines are previous assessments.[2,63] Experimental points are from.[64–69]

VI. CONCLUSION

A complete critical evaluation of all available phase diagram and thermodynamic data at 1 atm total pressure for the Ca-Fe-O system has been carried out, and a database of optimized model parameters has been developed. A wide variety of available data are described by few model parameters. The most recent experimental data have been taken into account. In particular, the properties of $Ca_4Fe_9O_{17}$ (C4WF4) phase, the solubility of Ca in spinel, the miscibility gap in the wüstite-lime (monoxide) solution, and the lime liquidus at iron saturation have been re-evaluated.

With the present optimized database, it is possible to calculate any phase diagram section for all compositions and oxygen partial pressures. The current database provides the best presently available description of the thermodynamic properties and phase equilibria in the Ca-Fe-O system.

In the present study, the thermodynamic database for the oxide phases has been combined with the physically realistic model for the liquid Fe-Ca-O alloy, which may be used for the prediction of deoxidation of steels.

The thermodynamic database reported here can be combined with the earlier optimizations of other chemical systems[9,72–76] to produce a multicomponent database, which can be used in combination with the liquid matte solution[77–79] for many applications in pyrometallurgy, steel-making, development of new ceramic materials, and refractory linings.

Fig. 28—Liquidus projection of the CaO-FeO-Fe₂O₃ portion of the Ca-Fe-O phase diagram up to 2000 K (1727 °C). The formation of gas phase is suppressed. Experimental points[54,70] and calculated lines. The calculations of the present study are shown by the solid lines, and the calculations of Selleby and Sundman[2] are shown by the dashed lines.
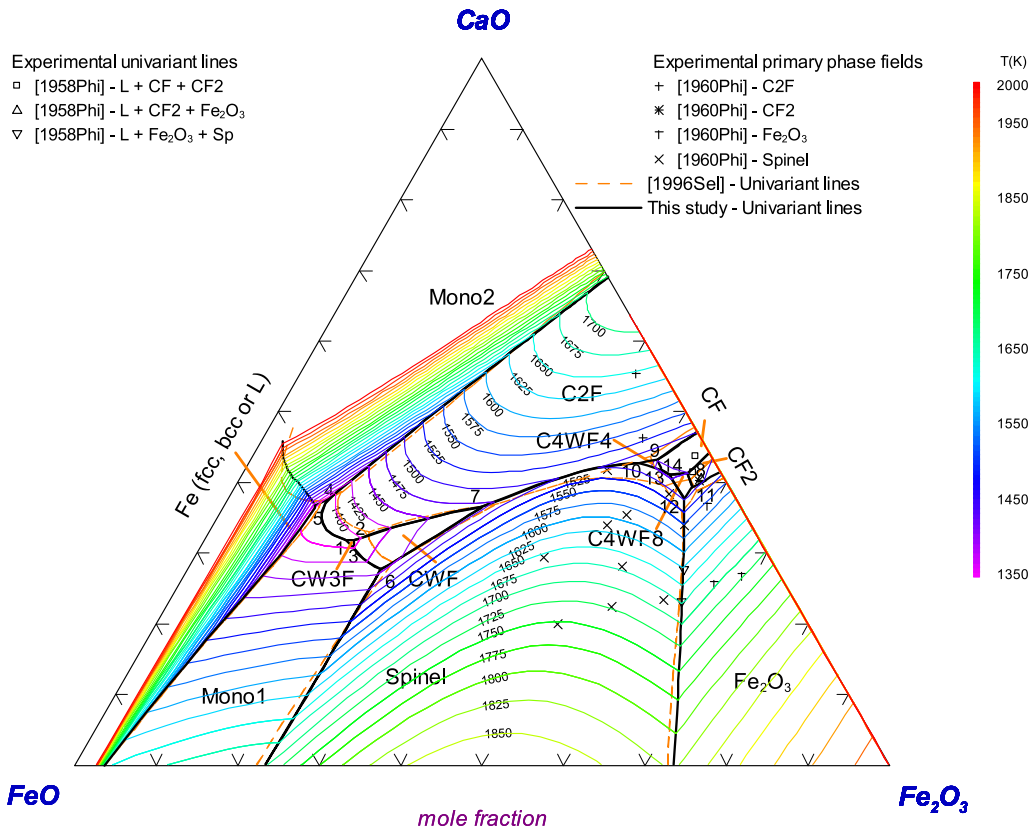
Table II. Invariant Points Involving Liquid Slag in the Ca-Fe-O System

	Reaction on Cooling	Experimental T [K (°C)]	Selleby and Sundman[2] T [K (°C)]	Present Study T [K (°C)]
1	L(Slag) + CW3F → C2F + Mono1	<1373 (<1100)[28]	1371 (1098)	1388 (1115)
2	L(Slag) + CWF → C2F + CW3F	1373 (1100)[28] >1387 (>1114)[31]	1374 (1101)	1392 (1120)
3	L(Slag) + Mono1 → CWF + CW3F	>1373 (>1100)[28]	1381 (1108)	1400 (1127)
4	L(Slag) + Mono2 → C2F + Mono1	—	1378 (1105)	1387 (1114)
5	L(Slag) + fcc(Fe) + Mono2 → Mono1	—	1404 (1131)	1403 (1130)
6	L(Slag) + Spinel → CWF + Mono1	—	1424 (1151)	1440 (1167)
7	L(Slag) + Spinel + C2F → CWF	—	1450 (1177)	1468 (1194)
8	L(Slag) + CF₂ → C4WF8 + CF	1473 (1200)[70]	1467 (1194)	1474 (1201)
9	L(Slag) + C2F → C4WF4 + CF	1483 (1210)[70]	1475 (1202)	1475 (1201)
10	L(Slag)→ Spinel + C2F + C4WF4	1485 (1212)[70]	1475 (1202)	1480 (1207)
11	L(Slag) + Fe₂O₃ → C4WF8 + CF2	1493 (1220)[70]	1486 (1213)	1488 (1215)
12	L(Slag) + Fe₂O₃ + Spinel → C4WF8	1503 (1230)[70]	1505 (1232)	1496 (1223)
13	L(Slag) + C4WF4 → CF + Spinel	1470 (1197)[70]	1460 (1187)	1471 (1199)
14	L(Slag) → CF + C4WF8 + Spinel	1467 (1194)[70]	1460 (1187)	1470 (1197)

Table III. Optimized Model Parameters for the Liquid and Solid Phases in the Ca−Fe−O System

Compounds	Temperature range (K) and reference	$\Delta H^o_{298.15}$, kJ mol^{-1}	$S^o_{298.15}$, J mol^{-1} K^{-1}	$C_p(T)$, J mol^{-1} K^{-1}
CaO	298.15 to 2900[71]	−635.299	37.750	58.791 − 1147146.0T^{-2} − 133.904$T^{-0.5}$ + 10298786.0T^{-3}
Fe$_2$O$_3$	298.15 to 2500[8]	−809.082	105.935	137.009 − 2907640T^{-2}
CaFe$_2$O$_4$ (CF)	298.15 to 2000	−1479.000	145.000	170.988 + 0.016000T − 1818972.0T^{-2}
Ca$_2$Fe$_2$O$_5$ (C2F)	298.15 to 2000	−2127.150	189.900	245.085 + 0.004877T − 4799514.6T^{-2}
CaFe$_5$O$_5$ (CWF)	298.15 to 2500	−1740.700	220.455	234.800 + 0.014790T − 3682800.0T^{-2}
CaFe$_4$O$_7$ (CF2)	298.15 to 2500	−2241.100	283.000	325.990 + 0.002326T − 6761000.0T^{-2}
CaFe$_5$O$_7$ (CW3F)	298.15 to 2500	−2267.350	344.828	344.180 + 0.025303T − 4981000.0T^{-2}
Ca$_4$Fe$_9$O$_{17}$ (C4WF4)	298.15 to 2500	−6217.375	636.079	809.970 + 0.014886T − 16128000.0T^{-2}
Ca$_4$Fe$_{17}$O$_{29}$ (C4WF8)	298.15 to 2500	−9255.047	1203.483	1358.300 + 0.014673T − 27787000.0T^{-2}

Solutions	Temperature Range (K) and Reference	Molar Gibbs Energy $g(T)$, J mol^{-1}
Spinel		compound energy formalism: $(Fe^{2+}, Fe^{3+})[Fe^{2+}, Fe^{3+}, Ca^{2+}, Va]_2^O O_4^{2-}$
Fe–O parameters	[8]	
$G_{(Fe^{4+})^{tetr}[Ca_{0.5}^{2+}Fe_{0.5}^{3+}]^{oct}O_4^{-2}}$		−1480266.3 + 997.1104T − 170.9880Tln$T$ − 0.0080000T^2 + 909486.0T^{-1} + 2RTln0.5
$\Delta_{Fe^{3+}Fe^{2+}Fe^{2+}Ca^{2+}}$		0
Wüstite–Lime solid solution (monoxide)		Bragg–Williams random mixing: (FeO, FeO$_{1.5}$, CaO); Kohler-type extrapolation of binary parameters into ternary system
g_{FeO}, $g^o_{FeO_{1.5}}$	[8]	
$q^{11}_{FeO,FeO_{1.5}}$, $q^{21}_{FeO,FeO_{1.5}}$	[8]	16526.8 + 2.8033T
$q^{11}_{CaO,FeO}$		15480.8 − 1.4943T
$q^{21}_{CaO,FeO}$		8368.0
$q^{11}_{CaO,FeO_{1.5}}$		
Liquid slag (CaO-FeO-Fe$_2$O$_3$)		Modified Quasichemical Model: $(Fe^{2+}, Fe^{3+}, Ca^{2+})(O^{2-})$; Toop-type extrapolation with Fe$_2$O$_3$ as asymmetrical component
$Z^{Fe^{2+}}_{Fe^{2+}Fe^{2+}} = Z^{Ca^{2+}}_{Ca^{2+}Ca^{2+}} = Z^{Ca^{2+}}_{Ca^{2+}Fe^{2+}} = Z^{Fe^{2+}}_{Fe^{2+}Ca^{2+}} = 1.37744375, Z^{Fe^{3+}}_{Fe^{3+}Fe^{3+}} = 2.06616563,$	[9]	
g^o_{FeO}	[9]	
$g^o_{Fe_2O_3}$	298.15 to 2845	
g^o_{CaO}	[9]	−571766.7 + 348.7358T − 58.7912Tln$T$ + 573573.0T^{-1} − 535.6160$T^{0.5}$ − 17163131.3T^{-2}
$q^{01}_{Fe^{2+},Fe^{4+}}$, $q^{20}_{Fe^{2+},Fe^{3+}}$		−38074.4
$\Delta g^o_{Ca^{2+},Fe^{2+}}$		−13807.2
$g^{01}_{Ca^{2+},Fe^{2+}}$		−74684.4
$\Delta g^o_{Ca^{2+},Fe^{3+}}$		−94976.8 + 27.1960T
$g^{01}_{Ca^{2+},Fe^{3+}}$		12552.0
$g^{10}_{Ca^{2+},Fe^{3+}}$		−43932 + 31.3800T
$g^{20}_{Ca^{2+},Fe^{3+}}$		−135846.1 + 66.9440T
$q^{11}_{Fe^{3+},Ca^{2+}(Fe^{2+})}$ (Bragg–Williams)		−66379.2 + 20.9200T
$q^{011}_{Fe^{2+},Ca^{2+}(Fe^{3+})}$ (Quasichemical)		
Liquid metal (Ca-Fe-O)		Bragg–Williams: (Fe, Ca, O, CaO); Mugianu-type extrapolation of binary parameters into ternary system

Table III. continued

Solutions	Temperature Range (K) and Reference	Molar Gibbs Energy $g(T)$, J mol^{-1}
g_{Fe}°, g_O°	[9]	
g_{Ca}°	298.15 to 500	$5844.8 + 62.4838T - 16.31387T\ln T - 0.01110455T^2 - 133574T^{-1}$
	500 to 1115	$7838.9 + 18.2979T - 8.9875T\ln T - 0.02266537T^2 - 230193T^{-1} + 3.338303\cdot10^{-6}T^3$
	>1115	$-2654.9 + 188.9223T - 35.0000T\ln T$
g_{CaO}°	298.15 to 2500	$-142268.7 + 12.4763T - 35.7704T\ln T - 0.00104600T^2 + 41840T^{-1}$
	>2500	$-148739.3 + 53.2713T - 40.9870T\ln T$
$L_{Fe,Ca}^0$		120233.0
$L_{Ca,CaO}^0$		$-291020.4 + 32.5422T$
fcc (solid metal)		Bragg–Williams (Fe, Ca, O)
$g_{Fe}^\circ, g_O^\circ, L_{Fe,O}^0$	[8]	
g_{Ca}°	298.15 to 1115	$-4955.1 + 72.7943T - 16.3138T\ln T - 133574.0T^{-1} - 0.011104557T^2$
	>1115	$-107304.4 + 799.9821T - 114.2922T\ln T$ $-18245540.0T^{-1} - 0.0237338147T^2 - 1.2438\cdot10^6T^3$
$L_{Fe,Ca}^0$		120705.0
bcc (solid metal)		Bragg–Williams (Fe, Ca, O)
$g_{Fe}^\circ, g_O^\circ, L_{Fe,O}^0$	[8]	
g_{Ca}°	298.15 to 716	$-7020.9 + 142.9702T - 28.2541T\ln T + 60578.0T^{-1} + 0.0072326T^2 - 4.5002\cdot10^6T^3$
	716 to 1115	$1640.5 + 2.0000T - 6.2760T\ln T - 523000.0T^{-1} - 0.0161921T^2$
	>1115	$-142331.1 + 1023.5490T - 143.8727T\ln T + 25355771.0T^{-1} + 0.032543127T^2 - 1.70408\cdot10^6T^3$
$L_{Fe,Ca}^0$		120705.0

REFERENCES

1. M. Hillert, M. Selleby, and B. Sundman: *Metall. Trans. A*, 1990, vol. 21, pp. 2759–76.
2. M. Selleby and B. Sundman: *Calphad*, 1996, vol. 20, pp. 381–92.
3. S. Ban-Ya, Y. Iguchi, H. Ishizuka, T. Shibata, and M. Arai: in *3rd International Conference on Molten Slags and Fluxes,* 27–29 June, 1988, 1989. University of Strathclyde, Glasgow.
4. E. Rosen and B. Saitton: *Scand. J. Metall.*, 1995, vol. 24, pp. 176–79.
5. H.-Y. Li and X.-M. Guo: *Metall. Mater. Trans. B*, 2015, vol. 46, pp. 278–85.
6. M. Aspiala, T. Hidayat, P. Taskinen, and E. Jak: *J. Alloys. Compd,* 2015. doi:10.1016/j.jallcom.2015.10.280.
7. C.W. Bale, E. Belisle, P. Chartrand, S.A. Decterov, G. Eriksson, K. Hack, I.-H. Jung, Y.-B. Kang, J. Melancon, A.D. Pelton, C. Robelin, and S. Petersen: *Calphad*, 2009, vol. 33, pp. 295–311.
8. T. Hidayat, D. Shishin, E. Jak, and S. Decterov: *Calphad*, 2015, vol. 48, pp. 131–44.
9. D. Shishin, V. Prostakova, E. Jak, and S. Decterov: *Metall. Mater. Trans. B*, submitted, 2015.
10. D.J.M. Bevan, and F.D. Richardson: *Proc. Aust. Atomic Energy Symp. on the Peaceful Uses of Atomic Energy*, 1958, Melbourne University Press, Melbourne, Australia, 1959, 1958, pp. 586–87.
11. H.A. Wriedt: *Bull. Alloy Phase Diagr.*, 1985, vol. 6, pp. 337–42.
12. J.C. Anglezio, C. Servant, and I. Ansara: *Calphad*, 1994, vol. 18, pp. 273–309.
13. A.D. Pelton: *Calphad*, 2001, vol. 25, pp. 319–28.
14. S.A. Decterov, E. Jak, P.C. Hayes, and A.D. Pelton: *Metall. Mater. Trans. B*, 2001, vol. 32, pp. 643–57.
15. M. Hillert and L.-I. Staffansson: *Acta Chem. Scand.*, 1970, vol. 24, pp. 3618–26.
16. M. Hillert, B. Jansson, and B. Sundman: *Z. Metallkd.*, 1988, vol. 79, pp. 81–87.
17. M. Hillert and M. Jarl: *Calphad*, 1978, vol. 2, pp. 227–38.
18. A.D. Pelton, S.A. Decterov, G. Eriksson, C. Robelin, and Y. Dessureault: *Metall. Mater. Trans. B*, 2000, vol. 31, pp. 651–59.
19. A.D. Pelton and P. Chartrand: *Metall. Mater. Trans. A*, 2001, vol. 32, pp. 1355–60.
20. E. Jak: in *Unpublished Work: Centre de Recerce en Calcul Thermochimique (CRCT), École Polytechnique, Montréal, Québec.* 1999.
21. E.G. King: *J. Am. Chem. Soc.*, 1954, vol. 76, pp. 5849–50.
22. K.V. Rajagopalan, R. Prasad, R. Kalyanaraman, and M. Sundaresan: *J. Therm. Anal.*, 1991, vol. 37, pp. 2253–58.
23. K.R. Bonnickson: *J. Am. Chem. Soc.*, 1954, vol. 76, pp. 1480–82.
24. T.N. Rezukhina and Y. Bagin'ska: *Elektrokhimiya*, 1967, vol. 3, pp. 1146–49.
25. K.T. Jacob, N. Dasgupta, and Y. Waseda: *Z. Metallkd.*, 1999, vol. 90, pp. 486–90.
26. S. Forsberg, P. Wikstrom, and E. Rosen: *Metall. Mater. Trans. B*, 2002, vol. 33, pp. 385–92.
27. D.A. Reeve and A.G. Gregory: *Inst. Min. Metall. Trans. Sect. C*, 1967, vol. 76, pp. 268–77.
28. B. Bergman and C. Song: *J. Am. Ceram. Soc.*, 1989, vol. 72, pp. 1364–67.
29. W.S. Chung, T. Murayama, and Y. Ono: *Kogaku Shuho—Kyushu Daigaku*, 1989, vol. 62, pp. 133–40.
30. W.S. Chung, T. Murayama, and Y. Ono: *Trans. ISIJ*, 1988, vol. 28, p. B-4.
31. W.S. Chung, T. Murayama, and Y. Ono: *Nippon Kinzoku Gakkaishi*, 1988, vol. 52, pp. 973–80.

32. V.B. Tare and B. Deo: *Montpellier*, 1975, vol. 3, pp. 104–13.
33. B. Bjorkman: *Scand. J. Metall.*, 1984, vol. 13, pp. 193–200.
34. A. Burdese and C. Brisi: *Ricerca Sci.*, 1952, vol. 22, pp. 1564–67.
35. A.A. Lykasov and N.V. Kozheurova: *Izv. Akad. Nauk SSSR, Neorg. Mater.*, 1980, vol. 16, pp. 1079–82.
36. G. Malquori and V. Cirilli: *Gazzetta Chimica Italiana*, 1945, vol. 75, pp. 137–56.
37. P. Perrot: *Rev. Chim. Miner.*, 1967, vol. 4, pp. 465–93.
38. S. Nikolic, P.C. Hayes, and E. Jak: *Metall. Mater. Trans. B*, 2009, vol. 40, pp. 900–09.
39. Y. Takeda, S. Nakazawa, and A. Yazawa: *Can. Metall. Q.*, 1980, vol. 19, pp. 297–305.
40. W. Oelsen and H. Maetz, *Mitt. Kaiser-Wilhelm Inst. Eisenforsch.*, 1941, vol. 23, pp. 195–245.
41. F. Abbattista, A. Burdese, and M. Maja: *Rev. Int. Hautes Temp. Refract.*, 1975, vol. 12, pp. 337–42.
42. B. Zhao, E. Jak, and P. Hayes, *Experimental studies in Ca-Fe-O slag system.* Unpublished Work: Pyrometallurgy Research Centre, The University of Queensland, 2003.
43. H. Larson and J. Chipman: *J. Met.*, 1953, vol. 197, pp. 1089–96.
44. W.C. Allen and R.B. Snow: *J. Am. Ceram. Soc.*, 1955, vol. 38, pp. 264–80.
45. W.A. Fischer and H.J. Fleischer: *Arch. Eisenhuettenwes.*, 1961, vol. 32, pp. 305–13.
46. E. Görl, F. Oeters, and R. Scheel: *Arch. Eisenhuettenwes.*, 1966, vol. 37, pp. 441–45.
47. K.H. Obst, H.C. Horn, and J. Stradtmann: *Mikrochim. Acta, Suppl.*, 1968, vol. 3, pp. 147–54.
48. M. Timucin and A.E. Morris: *Metall. Trans.*, 1970, vol. 1, pp. 3193–3201.
49. S. Hara, T. Araki, and K. Ogino: in *Int. Symp. Proc. 2nd, 1984*. 1984. Metall. Soc. AIME, Warrendale.
50. R. Scheel: *Arch. Eisenhuttenwes.*, 1974, vol. 45, pp. 751–56.
51. S. Ban-Ya, A. Chiba, and A. Hikosaka: *J. Iron Steel Inst. Jpn.*, 1980, vol. 66, pp. 1484–93.
52. J. White: *Iron Steel Inst.*, 1938, vol. 27, pp. 1–75.
53. R.W. Gurry and L.S. Darken: *J. Am. Chem. Soc.*, 1950, vol. 72, pp. 3906–10.
54. B. Phillips and A. Muan: *J. Am. Ceram. Soc.*, 1958, vol. 41, pp. 445–54.
55. J.O. Edstroem: *Jernkontorets Ann.*, 1956, vol. 40, pp. 101–15.
56. P. Batti: *Chim. Ind. (Milan, Italy)* 1956, vol. 38, pp. 864–66.
57. X.G. Liu: in *School of Chemical Engineering*. 2012, University of Queensland, Brisbane, pp. 108.
58. R.E. Johnson and A. Muan: *Trans. Met. Soc. AIME*, 1967, vol. 239, p. 1931.
59. M. Iwase, N. Yamada, K. Nishida, and E. Ichise: *Trans. Iron Steel Soc. AIME*, 1984, vol. 4, pp. 69–75.
60. D.R. Chang and R.A. Howald: *High Temp. Sci.*, 1982, vol. 15, pp. 209–18.
61. J. Berggren: *I Exp. Scand. J. Metall.*, 1975, vol. 4, pp. 75–80.
62. J. Berggren: *Scand. J. Metall.*, 1975, vol. 4, pp. 140–44.
63. I.-H. Jung, S.A. Decterov, and A.D. Pelton: *Metall. Mater. Trans. B*, 2004, vol. 35, pp. 493–507.
64. T. Ototani, Y. Kataura, and T. Degawa: *Trans. Iron Steel Inst. Jpn.*, 1976, vol. 16, pp. 275–82.
65. S. Gustafsson and P.O. Mellberg: *Scand. J. Metall.*, 1980, vol. 9 (3), pp. 111–16.
66. J.-D. Seo and S.-H. Kim: *Bull. Kor. Inst. Metall. Mater. (Korea)*, 1999, vol. 12, pp. 402–11.
67. Y. Miyashita and K. Nishikawa: *Tetsu to Hagane*, 1971, vol. 57, pp. 1969–75.
68. Q. Han, X. Zhang, D. Chen, and P. Wang: *Metall. Trans. B*, 1988, vol. 19, pp. 617–22.
69. M. Ozawa: The Japan Society for the Promotion of Science, 19th Committee paper No. 9837, Iron Steel Institute of Japan, Tokyo, 1975, p. 6.
70. B. Phillips and A. Muan: *Trans. Am. Inst. Min. Metall. Eng.*, 1960, vol. 218, pp. 1112–18.
71. G. Eriksson and A.D. Pelton: *Metall. Trans.*, 1993, vol. 24, pp. 807–16.
72. I.-H. Jung, S.A. Decterov, and A.D. Pelton: *J. Phase Equilib.*, 2004, vol. 25 (4), pp. 329–45.
73. D. Shishin, T. Hidayat, E. Jak, and S. Decterov: *Calphad*, 2013, vol. 41, pp. 160–79.
74. I.-H. Jung, Y.-B. Kang, S.A. Decterov, and A.D. Pelton: *Metall. Mater. Trans. B*, 2004, vol. 35, pp. 259–68.
75. I.-H. Jung, S.A. Decterov, and A.D. Pelton: *J. Phys. Chem. Solids*, 2004, vol. 65, pp. 1683–95.
76. I.-H. Jung, S.A. Decterov, and A.D. Pelton: *J. Am. Ceram. Soc.*, 2005, vol. 88, pp. 1921–28.
77. D. Shishin and S.A. Decterov: *Calphad*, 2012, vol. 38, pp. 59–70.
78. D. Shishin, E. Jak, and S.A. Decterov: *J. Phase Equilib. Diff.* 2015.
79. D. Shishin, E. Jak, and S.A. Decterov: *Calphad*, 2015, vol. 50, pp. 144–60.